


Polarization Orientation in Lead Zirconate Titanate (001) Thin Films Driven by the Interface with the Substrate

Liviu C. Tănase,^{1,2} Laura E. Abramiuc,^{1,2} Dana G. Popescu,¹ Ana-Maria Trandafir,¹
Nicoleta G. Apostol,¹ Ioana C. Bucur,^{1,2} Luminița Hrib,¹ Lucian Pintilie,¹ Iuliana Pasuk,¹
Lucian Trupină,¹ and Cristian M. Teodorescu^{1,*}

¹National Institute of Materials Physics, Atomiștilor 405A, 077125 Măgurele–Ilfov, Romania

²Faculty of Physics, University of Bucharest, Atomiștilor 405, 077125 Măgurele–Ilfov, Romania

 (Received 16 August 2017; revised manuscript received 5 April 2018; published 11 September 2018)

We investigate the effect of the nature of the substrate and the bottom interface on the out-of-plane polarization orientation of ultrathin (10-nm) lead zirconate titanate (PZT) thin films of (001) orientation by photoelectron spectroscopy of samples without surface contamination. The substrate nature is varied between insulator (strontium titanate, STO) and semiconductor (Nb-doped STO, STON) and finally to a metal with a work function lower than that of PZT (strontium ruthenate, SRO). Outward polarization is obtained for PZT/STON(001) and inward polarization is obtained for PZT/STO(001) and PZT/SRO(001). Explanations are given for all these typical cases, the main elements being charge accumulation for compensation of the depolarization field, self-doping of PZT films, and the interface electric field driving the orientation of the polarization of the ferroelectric films. We find *p*-type self-doping is correlated with the inward polarization, and the driving field is formed between a negatively charged region with negatively ionized acceptors near the interface with the substrate and the *p*-type degenerate region with holes accumulated inside, toward the surface. This mechanism may be reversed under the assumption of *n*-type self-doping, positively ionized donors near the interface, and accumulated electrons toward the surface in the case of an interface with a substrate with a higher work function, being in line with recent data (PZT/Pt or BaTiO₃/SRO).

DOI: [10.1103/PhysRevApplied.10.034020](https://doi.org/10.1103/PhysRevApplied.10.034020)

I. INTRODUCTION

In recent years there have been considerable advances in the field of ferroelectric single crystals and thin ferroelectric films grown epitaxially on different substrates. Before thinking about applications of ferroelectrics in the field of nonvolatile memories [1], piezoelectric devices [2], gas sensors [3,4], catalysis [5–9], photocatalysis [10,11], or photovoltaic applications [12,13], including selectivity for molecular adsorbates [8,14,15] or interfaces with graphene [16,17] for memristors, one should try to elucidate the mechanisms causing the establishment of out-of-plane polarization states. For an ultrathin ferroelectric layer with polarization $P \approx 1 \text{ cm}^{-2}$ and dielectric constant around 100, the depolarization field is on the order of 10^9 V m^{-1} , several orders of magnitude higher than coercive fields in usual ferroelectrics of about 10^7 V m^{-1} [18,19]. This field is oriented antiparallel to the polarization and would imply the destruction of the single-domain out-of-plane polarization state, unless inside the ferroelectric thin film a charge-compensation mechanism intervenes [20,21]. Ferroelectric

materials are wide-band-gap semiconductors, but by convenient doping they may provide sufficient charge carriers to compensate the depolarization field [19]. Alternatively, charge carriers may be provided by the bottom electrode if the ferroelectric material is synthesized on a metal with convenient lattice matching; for example, SrRuO₃ (SRO) (001) or Pt(001) for Pb(Zr,Ti)O₃ (PZT) [19]. Also, for electrical measurements the ferroelectric layers are sandwiched between metals, and image charges may be created in the metals also to compensate the depolarization field. Figure 1 presents a summary of possible mechanisms of charge compensation, either intrinsic [Fig. 1(a)] or extrinsic [Fig. 1(b)].

Alternatively, free ferroelectric surfaces exposed to ambient conditions attract contaminant molecules from the environment [14,15] and compensation charges may be created inside this contaminating layer (i.e., outside the ferroelectric) [7,11]. It is then of prime importance to work in the absence of contaminants to see exactly which is the intrinsically stable ferroelectric state.

The field of ordered ferroelectric ultrathin layers with well-defined polarization has grown exponentially in recent years. Here we present a systematic study of the orientation of out-of-plane polarization in ultrathin

*teodorescu@infim.ro

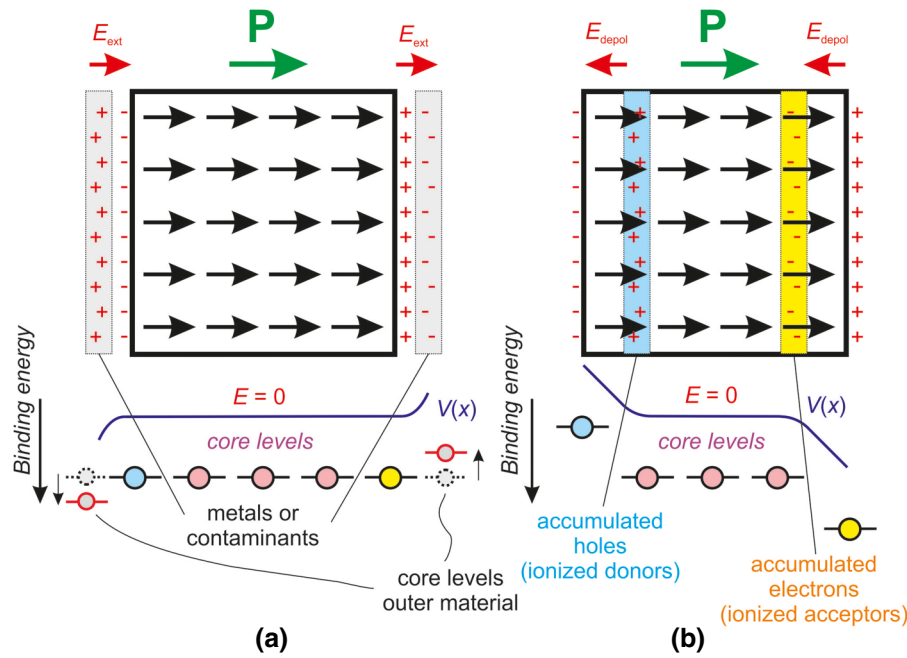


FIG. 1. Establishment of sheets of compensating charges, the electronic-potential-energy dependence $V(x)$ across a ferroelectric thin film with polarization \mathbf{P} oriented out of the plane, and principle of investigation of the polarization state by core-level X-ray photoelectron spectroscopy. (a) The case of a free material. Charge sheets, which may be mobile charge carriers or ionized impurities, are located near the surface to compensate the fixed charges due to ferroelectric polarization, represented as red + and - signs on the surfaces. The depolarization field E_{depol} manifests itself only in restricted regions between the surface and the charge sheets. This produces potential-energy variations near the surfaces that manifest themselves in variation of surface core-level positions, as measured by X-ray photoelectron spectroscopy. (b) The case of a material with metal contacts or with adsorbed contamination layers. In this case, it may happen that the compensating-charge sheets are formed outside the ferroelectric material itself. By X-ray photoelectron spectroscopy, core levels from the substrate may not show any variation in binding energies, but instead core levels from the outer material may show shifts opposed to those of core levels from the material in case (a), for the same polarization, because in this case the nonvanishing field outside the material E_{ext} is opposed to the depolarization field.

ferroelectric (PZT) films grown on different substrates. We start first with the presentation of experimental results, and then we build models to explain the polarization orientation in all cases: insulating, semiconducting, or metal substrates. An influence of the substrate properties (work function, conduction properties, dielectric constant) on the orientation of the polarization is supposed nowadays by several noticeable scientists in the field, yet experimental evidence is rather scarce, with some exceptions [22,23]. The possible outcomes of such a study are of high interest for many applications, including the following:

(a) Catalysis: ferroelectric surfaces with different out-of-plane polarizations $P^{(\pm)}$ have different oxidation ($P^{(-)}$) or reduction ($P^{(+)}$) activities.

(b) Photocatalysis: in addition to the catalytic properties, the surface depolarization field is effective in increasing charge separation and thus inhibiting recombination.

(c) Photovoltaics: again, for use of ferroelectrics in photovoltaic applications, one needs to identify surface or interface regions with electric fields able to cause charge separation, which emerge from our data and from the models we propose.

(d) Ferroelectric-based electronics: since the orientation of the polarization imprint depends on the doping or charge state of the substrate, one may modify the polarization state of the memory element via the substrate.

(e) Pyroelectric detectors: the efficiency of these elements is highly dependent on the ability to synthesize single-domain states.

For instance, in the case of PZT synthesized on SRO(001), working in ultraclean conditions yielded films with polarization oriented inward—that is, from the ferroelectric toward the metal substrate ($P^{(-)}$) [8,24]—while for PZT synthesized on Pt(001) the polarization was oriented outward ($P^{(+)}$) [17]. PZT on $(\text{La,Sr})\text{MnO}_3$ (LSMO) also exhibited inward built-in polarization [24]. In the presence of contaminants [i.e., under air, without ultrahigh-vacuum (UHV) conditions], the 20 nm-thick films reported in Ref. [8] presented $P^{(+)}$ polarization. The “self-doping” mechanism discussed in Ref. [19] to generate enough charge carriers for ultrathin films such that the compensating-charge surface density becomes comparable to the value of the polarization should work for both p -type and n -type doping; however, the easiest way to dope an oxide

is *n*-type doping, by creation of oxygen vacancies. Nevertheless, the above observation with different polarization states when ferroelectric layers are synthesized on different metals suggests that the setup of the polarization during the synthesis of the thin film might be related to the work function difference between the metal and the ferroelectric semiconductor.

A few years ago a remarkable work related the orientation of the polarization to atomic details of interface formation; namely, if a ferroelectric perovskite $A^{(1)}B^{(1)}O_3$ is grown on a perovskite substrate $A^{(2)}B^{(2)}O_3$, structures such as $\dots/A^{(2)}O/B^{(2)}O_2/A^{(1)}O/B^{(1)}O_2/\dots$ and $\dots/B^{(2)}O_2/A^{(2)}O/B^{(1)}O_2/A^{(1)}O/\dots$ should yield opposite polarization orientation owing to “interfacial valence mismatch” [25]. This work reported mainly BiFeO₃ (BFO) grown on LSMO, but similar effects were obtained also for BFO/SRO, BFO grown on Nb-doped SrTiO₃ (STON) (001), and PZT/LSMO, the last case being at variance with results from Ref. [24]. However, no comments were provided in Ref. [25] about the surface cleanliness, especially during the a posteriori testing of ferroelectric properties. Supposing, however, that the control of the overall ferroelectric polarization is governed by the stacking valence mismatch, the question arising is whether there are also some other interface aspects governing the orientation of the polarization, especially when such accurate stacking control at the single-atomic-layer level is not achievable.

Another recent work on ultrathin films of Pb(Mg_{1/3}Nb_{2/3})O₃-PbTiO₃ (PMN-PT) relaxor ferroelectrics reported P⁽⁺⁾ orientation of PMN-PT when it is grown on a half metal with a higher work function (La_{0.7}Sr_{0.3}MnO₃), and P⁽⁻⁾ orientation when it is grown on STON and SRO, both having a lower work function [22]. The explanation took into account the formation of an interface dipole associated with the Schottky barrier, oriented from the substrate toward PMN-PT in the case of a substrate with a higher work function ($\Phi_{\text{sub}} > \Phi_{\text{PMN-PT}}$), where the interface is formed by electron migration from the semiconductor (PMN-PT) to the metal, together with formation of an electron-depleted layer that may extend over the whole thickness of the semiconductor. This interface dipole further yields the *outward* polarization of the whole PMN-PT. In the case of a substrate with a lower work function ($\Phi_{\text{sub}} < \Phi_{\text{PMN-PT}}$), the interface dipole would consist of electron accumulation inside PMN-PT and electron depletion inside the substrate, with the interface dipole oriented from PMN-PT toward the substrate, and, as a consequence, the final orientation of the polarization is *inward*. It is, however, difficult to imagine how the interface dipole, produced by mobile-charge accumulation, may yield a further polarization of the material in the same direction. Rather, the interface electric field is oriented *inward* in the first case ($\Phi_{\text{sub}} > \Phi_{\text{PMN-PT}}$) and *outward* in the second case ($\Phi_{\text{sub}} < \Phi_{\text{PMN-PT}}$). This should yield polarization of the material with the dipoles oriented parallel to the

interface field, such that the depolarization field would cancel the field generated by mobile-charge accumulation (i.e., exactly the opposite of what is observed). For an interface dipole to polarize further the upper layers, one should take into account the field generated *outside* the region of the interface (i.e., to consider any other possible charge accumulation away from the barrier region, near the surface of the ferroelectric). In this paper, we try to analyze such data and give a quantitative explanation of this phenomenon.

Still not well studied is the ferroelectric polarization when a ferroelectric thin film is synthesized on another semiconductor or even on an insulator, such as PZT on SrTiO₃ (STO) (001) or PZT on STON, with the exception of Ref. [22] for PMN-PT/STON and Refs. [26–28] for PbTiO₃/STO. In such cases, we should not expect a consistent contribution from the substrate in terms of compensating charge carriers and then the “self-doping” mechanisms should prevail. Recently, it was reported that for thick layers (more than 200 nm), the depolarization field with less-effective compensation for PZT grown on relatively-low-doped STON (0.5% Nb) yields the formation of 180° domains, with a strong decrease of its pyroelectric coefficient [23]. The problem in such cases is to find a method to capture the polarization of the material, since electrical measurements implying metal contacts are excluded. Also, piezoresponse force microscopy (PFM) based on poling in a controlled way different areas of the surface and by a posteriori comparison of the PFM phase from unpoled regions with phases of the poled regions with known orientations [22] will scarcely work, since the necessary voltages are too elevated (one needs to apply a voltage to the film and substrate instead of the film only, and there are 5–6 orders of magnitude between the respective thicknesses, so for the same poling film one needs considerably higher voltages).

Fortunately, another method, X-ray photoelectron spectroscopy (XPS) is able to yield the surface polarization of free ferroelectric thin films [8,19,29–32] and of their interfaces with metals [18,33–38]. This method supposes a rigid shift of core levels of near-surface atoms, according to the shift manifested by the incomplete compensation of the depolarization field near the surface (see Fig. 1). There are also some limitations of this method, especially when surfaces are contaminated or electrodes are deposited on top; in this case, an extrinsic mechanism could hinder the intrinsic one, and evaluation with core levels from the ferroelectric material itself is less sensitive to the orientation of the polarization (see, e.g., Ref. [39]). XPS provides also compositions with surface sensitivity [29,30,34–36] and is a typical UHV technique; thus, the study of ferroelectric polarization of thin films without any back electrode is undertaken mainly by use this method, on the basis of extensive previous validations [8,15,17–19,29–38].

Consistent efforts were made during recent years regarding ab initio theoretical investigations of ferroelectric thin

films and of their interfaces. There is a clear interplay of detailed atomic structures (strain, octahedral rotations, stoichiometry changes) on the macroscopic properties of these materials [40], and even the nature of the termination films at interfaces have been shown to play a role in determining the orientation of the polarization [41,42], in line with the findings from Ref. [25]. Theoretical [43] and experimental [26–28] work pointed to the existence of ferroelectricity for ultrathin layers, starting with thickness corresponding to about three unit cells, about 1.2 nm.

In this paper, we present a systematic investigation by XPS of atomically clean PZT ultrathin layers (10 nm thickness), synthesized on insulators (STO), *n*-doped semiconductors (STON, with different Nb concentrations) and SRO (work function lower than that of PZT). All substrates are (001)-oriented single crystals exhibiting an in-plane lattice constant on the order of 3.9 Å, thus inducing a compressive in-plane strain and favoring the tetragonal distortion of PZT layers [44]. We conclude that the results cannot be ascribed to a single mechanism (e.g., the orientation of the interface field in setting the polarization), but they can be assessed by a wide variety of other phenomena, such as self-doping, charge migration, and electric fields at the interface. For instance, in Ref. [45], the outward polarization for Pt/BTO/STON is explained by a higher asymmetry in the band alignment for the inward-polarized state, which implies that in this case the depolarization field exceeds the coercive field. We give an explanation based solely on electronic grounds, which estimates band bendings and interface fields for the heterostructures in question, with contribution from quantum chemistry or density-functional theory. Similar explanations were given for tunneling electroresistance phenomena in Ref. [46]. We hope that, in spite of the inherent simplifications of such a macroscopic continuous model, a consistent picture will emerge about the role of the bottom interface in the direction of the out-of-plane polarization, and that such information will be of prime importance for foreseen applications in microelectronics, sensors, photovoltaics, or catalysis.

II. EXPERIMENTAL SECTION

Ten-nanometer-thick PZT samples are deposited by pulsed-laser deposition (PLD) using a KrF laser (wavelength 248 nm, repetition rate 5 Hz, pulse $0.7 \text{ J} \times 20 \text{ ns}$, laser fluence 2 J/cm^2) on STO(001), STON (0.05% Nb) (001), STON (0.5% Nb) (001), and SRO/STO(001) single crystals starting with PZT commercial targets enriched in PbO. PZT is deposited on Pt(001) with use of the same parameters; the complete procedure is described in Refs. [17,47]. The synthesis occurs at about 850 K. XPS is performed in an analysis chamber equipped with a 150-mm hemispherical electron-energy analyzer (Phoibos) with Al $K\alpha_1$ monochromatic radiation (1486.74 eV). Sample neutralization is achieved with a flood gun operating

at 1-eV electron energy and 100- μA electron current. Previous studies have reported the use of a flood gun [15,19,30–33,48]; its operating voltage and current are chosen after several series of calibration for its possible influence on core-level positions. The analyzer operated in fixed-transmission mode with pass energy of 20 eV; the estimated combined (source plus analyzer) resolution is about $0.750 \pm 0.025 \text{ eV}$. The energy is calibrated repeatedly with the Au $4f_{7/2}$ core level (83.81 eV) with use of separate thick Au depositions. After the introduction into the XPS chamber, the samples are measured with no other treatments. After the first measurement, the samples are annealed in UHV, up to a temperature $T \approx 400 \text{ }^\circ\text{C}$, and after that a second annealing is performed at $T \approx 400 \text{ }^\circ\text{C}$ in an O_2 atmosphere (0.005 Pa), following Refs. [8,49]. After the second annealing in an oxygen atmosphere, the samples exhibit negligible carbon contamination; see Fig. S5 in Supplemental Material (SOM) [50]. The base pressure during the measurements is around 10^{-7} Pa . C 1s spectra are recorded at the beginning and at the end of each measurement cycle for each sample and do not show noticeable differences.

In Supplemental Material [50] we present X-ray diffraction data obtained on these films before the XPS analysis, exhibiting the synthesis of highly strained tetragonal films, epitaxially grown on all substrates (Figs. S1-1 and S1-2 in Supplemental Material [50]). Atomic force microscopy (AFM; Sec. S2 from the Supplemental Material [50]) shows an atomically flat film, while PFM (Sec. S2 from the Supplemental Material [50]), when films could be out-of-plane poled, points to outward polarization, especially for PZT/SRO and PZT/STON (Fig. S2-2 in Supplemental Material [50]). This is an apparent contradiction for PZT/SRO, since XPS data for an ultraclean film reveal inward polarization, while PFM in air shows outward polarization. The contaminated PZT/SRO film also shows outward polarization by shifts of XPS spectra toward higher binding energy (see Fig. S4 in Supplemental Material [50]). The same was found for PZT/SRO films with greater thickness (20 nm) analyzed in Ref. [8]. For the moment, let us assume that this difference is mainly due to the contaminated or uncontaminated nature of the surface. Toward the end of this work, we will give an explanation for this phenomenon.

In Sec. S3 in Supplemental Material [50], we present low-energy-electron-diffraction (LEED) patterns for the cases where such patterns could be obtained (owing to the conduction properties of the substrate) for PZT/SRO and PZT/STON (0.5% Nb). More LEED data for films of different thicknesses, for both SRO and LSMO substrates, are discussed in Ref. [51]. For this work, we use the fact that films of good quality, certified by X-ray diffraction and by high-resolution (Sec. S1 from the Supplemental Material [50]) transmission electron microscopy [18,19]

could be prepared in ultrahigh vacuum without surface contamination and with ordered surfaces.

In Sec. S4 in Supplemental Material [50] we present XPS spectra for all samples, as introduced, after the first annealing in ultrahigh vacuum and after annealing in 5 mPa O₂. The C 1s spectra are shown in Fig. S5 in Supplemental Material [50]. There is no noticeable C 1s signal after annealing in oxygen. The noise level of these spectra is about 50 counts/s. From the analysis of the other spectra, an integral intensity of about 3000 (counts/s) eV is inferred for a one-monolayer signal, after normalization by XPS atomic sensitivity factors [52]. This implies a bare integral intensity of about 750 (counts/s) eV for C 1s by use of the atomic sensitivity factor of 0.25 for C 1s. By use of a linewidth of about 1 eV for a single component, the lower limit of carbon contamination of about 7% of a monolayer may be derived.

III. X-RAY PHOTOELECTRON SPECTROSCOPY

XPS spectra recorded for ultraclean samples, after the removal of any visible carbon contamination (i.e., carbon contamination below about 7% of a monolayer) are illustrated in Fig. 2. XPS spectra for as-introduced samples and for an intermediate stage of cleaning are presented in Sec. S4 from the Supplemental Material [50], while C 1s spectra are presented in Sec. S1 from the Supplemental Material [50]. The spectra are deconvoluted with use of Voigt functions (Lorentzian and Gaussian widths) with a distinct inelastic background for each component [53,54]. A minimum number of components is used to obtain a convenient fit. As demonstrated also in Ref. [34], when excited with Al K α , a Pb Auger M₅N₂N₂ feature is superposed on the Ti 2p region, and this is taken into consideration by a broad singlet line.

As outlined in Sec. I, the polarization state of a thin ferroelectric layer can be characterized by the chemical shift of the core levels, as detected by XPS [8,15,19,29–33]. Table I presents the binding energies and the significant atomic ratios obtained from the deconvolutions, along with the interpretation of the polarization state based on these values. At most, three components are needed to simulate well the experimental data, which can be ascribed to different out-of-plane polarization states: P⁽⁺⁾ (i.e., outward), P⁽⁰⁾ (i.e., in plane or no polarization at all), or P⁽⁻⁾ (i.e., inward). One polarization state dominates in all cases, and the binding energies of components with dominant intensity are also outlined in Table I. We mention also the dominant polarization state for each sample in Table I. In the case of STON substrates, the polarization is P⁽⁺⁾, whereas in Ref. [22], inward polarization (P⁽⁻⁾) was reported by PFM investigations.

The atomic concentration ratios presented in Table I are computed from the sums of integral intensities, by use of XPS atomic sensitivity factors [52]. The Zr-to-Ti

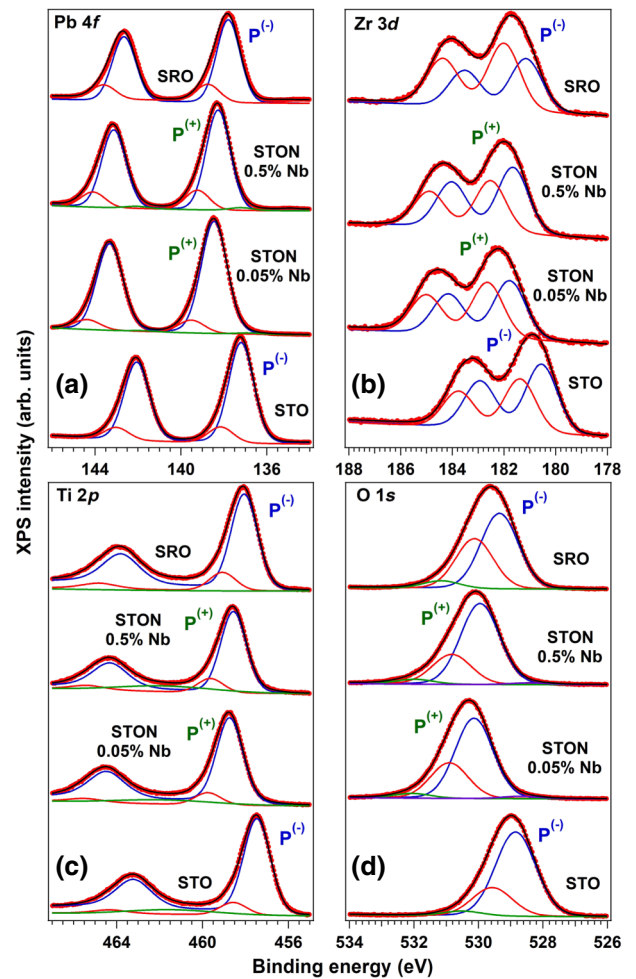


FIG. 2. Core-level X-ray photoelectron spectra for (a) Pb 4f, (b) Zr 3d, (c) Ti 2p, and (d) O 1s recorded for PZT/STO, PZT/STON (0.05% Nb), PZT/STON (0.5% Nb), and PZT/SRO/STO after annealing for 3 h first in ultrahigh vacuum, then in 5-mPa O₂ atmosphere. The spectra are deconvoluted with Voigt profiles; see the text for more details. Higher binding energies correspond to outward polarization P⁽⁺⁾, and lower binding energies correspond to inward polarization P⁽⁻⁾; see Fig. 1 for an explanation.

concentration ratios are close to the target composition, and the oxygen stoichiometry is reasonable; the Pb-to-Zr-plus-Ti concentration ratios are considerably lower than unity (below 0.7). Most probably, photoelectron-inelastic-mean-free-path and with photoelectron-diffraction effects contribute to this deviation. Nevertheless, for PZT/STON the ratios are close to each other, 0.69 ± 0.02 . The Pb-to-Zr-plus-Ti concentration ratios for PZT/STO and PZT/SRO are considerably lower than for PZT/STON (0.61 and 0.45, respectively). Thus, one may infer that in these films, at least in the last 2–3-nm outer layers, there is a Pb deficit, pointing to a *p*-type doping of these samples.

We discuss now the different components (separated by about 1.0 ± 0.2 eV) occurring in all Pb, Zr, Ti, and O spectra. These components are present in all spectra, no matter

TABLE I. Main parameters obtained from XPS of the samples whose spectra are presented in Fig. 1. Relevant atomic concentration ratios together with binding energies of the components obtained by deconvolution, normalized with respect to the major component (bold) for all cases. The last line represents the proposed polarization detected by XPS.

Parameter	PZT/STO (001)	PZT/STON(001) (0.05% Nb)	PZT/STON(001) (0.5% Nb)	PZT/SRO/ STO(001)
[Pb]:[Zr + Ti]	0.61	0.71	0.67	0.45
[Zr]:[Zr + Ti]	0.21	0.20	0.22	0.20
[O]:[Zr + Ti]	2.81	2.83	3.05	2.83
Pb $4f_{7/2}$ (c1) (eV); relative amplitude	137.20; 1.00	136.83; 0.01	137.16; 0.03	137.79; 1.00
Pb $4f_{7/2}$ (c2) (eV); relative amplitude	138.15; 0.16	138.45; 1.00	138.26; 1.00	138.72; 0.21
Pb $4f_{7/2}$ (c3) (eV); relative amplitude	(131.85)	139.51; 0.11	139.23; 0.20	...
Zr $3d_{5/2}$ (c1) (eV); relative amplitude	180.54; 1.00	181.77; 1.00	181.65; 1.00	181.14; 0.79
Zr $3d_{5/2}$ (c2) (eV); relative amplitude	181.37; 0.77	182.63; 0.95	182.51; 0.77	182.00; 1.00
Ti $2p_{3/2}$ (c1) (eV); relative amplitude	...	457.04; 0.01	456.96; 0.02	...
Ti $2p_{3/2}$ (c2) (eV); relative amplitude	457.46; 1.00	458.73; 1.00	458.56; 1.00	458.05; 1.00
Ti $2p_{3/2}$ (c3) (eV); relative amplitude	458.57; 0.13	459.75; 0.14	459.63; 0.18	459.06; 0.19
O $1s$ (c1) (eV); relative amplitude	...	528.69; 0.03	528.42; 0.02	...
O $1s$ (c2) (eV); relative amplitude	528.85; 1.00	530.14; 1.00	529.95; 1.00	529.35; 1.00
O $1s$ (c3) (eV); relative amplitude	529.57; 0.34	530.90; 0.44	530.82; 0.37	530.12; 0.66
O $1s$ (c4) (eV); relative amplitude	530.50; 0.06	532.05; 0.06	531.97; 0.06	531.15; 0.10
Polarization	p ⁽⁻⁾	p ⁽⁺⁾	p ⁽⁺⁾	p ⁽⁻⁾

whether the polarization is inward or outward. The effect of the polarization is a rigid shift of all components. Thus, the presence of two components is rather connected to the existence of two kind of atoms for each species rather than to polarization effects, at variance with the attempt to explain Ba $3d$ in Ref. [45]. This could be quite easily an effect of “surface reconstruction,” different positions for surface atoms as compared with atoms from deeper layers. The fact that two components with almost equal intensity are seen for Zr implies, for example, that some Zr atoms are displaced in the perovskite ABO_3 unit cell and others are not; according to Refs. [45,55] their dynamical (Callen) charge should be different, owing to different hybridizations with neighboring atoms. Indeed, the atomic diameter of Zr (about 3.1 Å) is close to the value of the diagonal of the unit cell (about 6.9 Å) minus twice the radius of Pb (3.6 Å), while the atomic diameter of Ti (2.8 Å) is considerably lower. As a consequence, one may conceive that Ti atoms have higher mobility, while some Zr atoms are displaced and some remain in centrosymmetric positions. Thus, Ti from the bulk has one major component, while Zr has two components with comparable amplitudes. Ti from the surface may have a lower rumpling, manifesting itself as the additional component with larger binding energy. In a similar way, Pb, for example, may have as a second-order neighbor a moving Zr (or a Ti) or a nonmoving Zr; if about half of the Zr atoms are not moving, the ratio between Pb with a neighboring centrosymmetric Zr and Pb with neighboring noncentrosymmetric Zr or Ti is about 1:9 to 1:11. It is also to be noted that in Ref. [8] only one component was sufficient for Ti and Zr, whereas Pb has a high-binding-energy component due to the PbO surface layer with incomplete oxygen coordination (these films were PbO

terminated). Also, these films were thicker (20 nm); therefore, the outer layers that are investigated are supposed to be more relaxed, allowing, for example, all Zr atoms to be displaced. In Ref. [50], also for 50-nm PZT/SRO and 100-nm PZT/LSMO, Ti and Zr were fitted with one component only, and, again, one may infer that these layers are relaxed, and all Ti and Zr cations are noncentrosymmetric. In the actual data, fitting Zr and Ti spectra with only one component did not provide reasonable results.

The attribution of the O $1s$ components, in this scenario, is as follows: The main component is attributed to bulk oxygen in the ferroelectric state; that is, belonging to unit cells with noncentrosymmetric B cations (Ti or Zr). The second component may be attributed to oxygen from the BO_2 surface layers, with reduced rumpling and thus atomic positions close to the centrosymmetric positions. The relative amplitude of this surface layer to the bulk component is approximately $\exp(c/\lambda) - 1 \approx 0.18$, where c is the lattice constant along the [001] direction (about 2 Å) and λ is the inelastic mean free path (about 12 Å for a kinetic energy of about 960 eV). The real ratio is higher, which means that there are also other contributions to this component. One possible contribution of similar binding energy would be oxygen coordinated to Zr atoms in centrosymmetric positions in the bulk. If one considers, again, similar probabilities for Zr to be centrosymmetric or noncentrosymmetric, simple statistical considerations of the possible coordination of oxygen in a BO_2 plane (B being Ti, Zr centrosymmetric or Zr noncentrosymmetric) yields a probability of oxygen having at least one centrosymmetric Zr neighbor of 0.3442 (if the probability that B is Zr is 0.2). With inelastic mean free path effects—that is, by use of an attenuation factor $\exp(-c/\lambda)$ —the relative

weight of this component to the main component becomes about 0.25. With both origins taken together for this component, it should be $0.18 + 0.25 \approx 0.43$ of the main component, which is close to the average value for all cases in Table I. If we take into account also the real ratio between the Zr highest- and lowest-binding-energy components, the total ratio of the second component to the first one becomes approximately 0.36, 0.41, 0.36, and 0.51 for PZT/STO, PZT/STON (0.05% Nb), PZT/STON (0.5% Nb), and PZT/SRO, values closer to the ones in Table I.

The third O 1s component, which is about 0.1–0.17 of the second one, may be ascribed to some oxygen from the last atomic layer (e.g., oxygen with more than one neighboring Zr atom). The attribution of O 1s components may be subject to some ambiguities, since one may easily compute that by adoption of the hypothesis of a ferroelectric bulk with two kind of Zr atoms and a surface layer with no rumpling, about 20 components are needed to account for all possible neighboring configurations of oxygen. Using so many components in the fit of course cannot yield reasonable results.

In any case, the above attribution of O 1s features is just a first sketch. The main purpose of our commenting on the different components obtained for XPS spectra of all elements is to evidence that these different components may be attributed to chemical, neighboring, or surface effects, without explicit use of charge accumulation or polarization. The effect of the polarization is a rigid shift of all core levels toward higher or lower binding energy, and the fact that this affects almost equally all components from all elements may be related to the extent of this band bending, which is considerably larger than the inelastic mean free path, about 16 Å for Pb 4f [34].

IV. DISCUSSION

To understand the processes that drive the stabilization of the out-of-plane polarization as function of the substrate, one needs to consider several physical parameters that can influence this process. Table II presents the relevant parameters of PZT and all substrates to understand interface band bending. In the following, we discuss every case to understand the information obtained from the XPS data.

It is important to note that the deposition temperature (about 850 K) corresponds to a transition from ferroelectric to paraelectric for films of about 7-nm thickness [26], the transition temperature becoming higher with greater film thicknesses [26,69]. Thus, thicker PZT films are grown in the ferroelectric state, whereas for the setting of the orientation of the polarization, one may reasonably start with films in the paraelectric state (or centrosymmetric state). The ferroelectric state is established by increase of the film thickness and/or lowering of the temperature,

but in any case at some early stage a thin paraelectric (centrosymmetric) film exists.

A. General aspects

A naive model supposes that when a ferroelectric semiconductor with a given work function is interfaced with another material with a different work function, the interface field will be oriented from the material with the lower work function toward the material with the higher work function. Suppose now that this interface field governs the orientation of the polarization, as supposed, for example, in Ref. [22]. In this case, PZT deposited on SRO (a metal with a lower work function) would develop an interface field oriented toward the PZT (i.e., outward), while PZT deposited on a metal with a higher work function (e.g., Pt) would develop an inward polarization. The data from Table I and Refs. [8,17,24,39,51,70,71] point to the opposite situation; see Fig. 3. Hence, this crude model must be refined by our taking into account charge transfer, self-doping [19], static charges created by ionized impurities, and variation of the work function with doping.

According to the previous sections and the existing literature on polarization orientation of thin ferroelectric films, the following basic assumptions are in order:

(a) All layers investigated in this work are strained to the lattice constant of the substrate (STO or STON). This is visible from the X-ray diffraction pattern (see Section S1 in Supplemental Material [50]) and also from recent reports [19]. Samples prepared in the same setup, by use of the same recipe, with thicknesses in the range from 5 to 250 nm, show that in-plane lattice relaxation starts by a film thickness of about 20 nm. Previous work reported the threshold for in-plane lattice relaxation as being around 30 nm for $\text{PbZr}_{0.48}\text{Ti}_{0.52}\text{O}_3$ [49]. Thus, a considerable tetragonal distortion of the unit cell is inherent to the epitaxial growth of the actual 10-nm-thick films, and the only question is what is the orientation of the polarization.

(b) The setting of the polarization orientation might be governed by the interface field with the substrate, which should exceed a value on the order of the coercive field. The coercive field is not a material constant; instead, for thin films it varies significantly. According to Ref. [19], the coercive field for 20-nm-thick PZT films is on the order of $(5-7) \times 10^7 \text{ V m}^{-1}$. It could be even higher for 10-nm-thick films. Suppose a centrosymmetric phase grows on a given substrate. When the interface field produced by charge transfer or accumulation (resulting in band bending) exceeds the coercive field, one supposes that the material will be poled in the direction of this interface field. This model is at variance with the naive model proposed in Ref. [22]. In this model, the interface dipole induces a polarization oriented in the *same* direction. It is not clear what the mechanism would be to align the polarization

TABLE II. Relevant parameters of PZT and of all substrates used in this work needed to quantify the interface band bending: band gaps, dielectric constants, and work functions.

Parameter	PZT	STO intrinsic	STON	SRO
Band gap E_g (eV)	3.4 [56]	3.25 (indirect); 3.75 (direct) [57]	3.25 (indirect); 3.75 (direct)	...
Dielectric constant ϵ_r	30–100 [51,59–62]	300 [58]	>300	∞ (metal)
Work function Φ (eV)	5.1–5.3 [18]5.35 [63]5.37–5.53 [64]5.8 [[65,66]]	4.2 [67]	<4.2	4.7–4.9 [18,22,68]5.21 [64]

orientation of the growing “polar nanoregions” parallel to the orientation of the interface dipole, since dipole-dipole interaction, in directions perpendicular to the dipole axes, tend to induce antiparallel orientation of interacting dipoles. Instead, what is important in this region is the “depolarization field” associated with the interface dipole, which is oriented antiparallel to this dipole.

(c) Thin films of ferroelectric materials undergo a “self-doping” to produce enough charge carriers to build up sheets of mobile charges that compensate the depolarization field in the volume of the field (Fig. 1). In Ref. [19], *n*-type self-doping was discussed, while in the actual case it seems that PZT/STO and PZT/SRO/STO (especially the latter) exhibit *p*-type self-doping manifested by the presence of Pb vacancies. *Films exhibiting p-type doping exhibit also inward polarization*, while surface-contaminated films from Ref. [19] exhibited *n*-type self-doping (oxygen vacancies) together with outward polarization. In the following, we assume that these charge sheets may be constituted also by ionized impurities; that is, even in the case of a single type of doping (*n* or *p*), mobile charge carriers may be accumulated at one extremity of the film, while ionized impurities of opposite sign may accumulate at the other extremity (see Fig. 1). In the case of the presence of a conductive or strongly doped material at one extremity (the substrate of the ferroelectric film), compensating charges needed at this extremity may be located also in this material. For compensating charges created in the ferroelectric material by defects, if ϵ_{def} is the energy needed for the creation of a defect in the material and N_{def}

is the density of these defects, the ferroelectric state (plus defects created) is stabler than the unpoled state without defects if its energy density is lower; that is,

$$\Delta w = -\frac{P^2}{2\epsilon(T)} + \epsilon_{\text{def}}N_{\text{def}} < 0, \quad (1)$$

where $\epsilon(T)$ is the (temperature-dependent) permittivity of the material. From here it follows there is an upper limit for the defect density, which for PZT at room temperature (polarization $P \approx 1 \text{ cm}^{-2}$) may be estimated as

$$\begin{aligned} N_{\text{def}} &< \frac{P^2}{2\epsilon(T)\epsilon_{\text{def}}} \\ &\approx \frac{1}{2 \times 8.8 \times 10^{-12} \times (60-150) \times 3 \times 1.6 \times 10^{-19}} \\ &\approx (0.8-2.0) \times 10^{27} \text{ m}^{-3}, \end{aligned} \quad (2)$$

with 60–150 being estimates of the PZT dielectric constant at room temperature [21,51], and 3 eV being an estimate of ϵ_{def} , valid both for oxygen vacancies (V_{O}) in the O-poor limit, or lead vacancies (V_{Pb}) near the valence band maximum in the O-rich limit [71]. The above inequality may be combined with the approximate density of unit cells (about $1.625 \times 10^{28} \text{ m}^{-3}$) to yield a maximum of 5.0%–12.5% defects per unit cell, on average. This is rather a large value in terms of doping, but is in line with the findings in Table I. An interesting evaluation may continue by stipulating the order of magnitude of the polarization is equal to

	insulator	semiconductor		metal
		<i>p</i> doped	<i>n</i> doped	
$\Phi_{\text{sub}} < \Phi_{\text{ferroel}}$	$P^{(-)}$	$P^{(-)}$	$P^{(+)}$	$P^{(-)}$
$\Phi_{\text{sub}} > \Phi_{\text{ferroel}}$	$P^{(+)}$	$P^{(+)}$	$P^{(-)}$	$P^{(+)}$

FIG. 3. Overview of the cases investigated in terms of work-function differences between the substrate and the ferroelectric film, and also as a function of the conduction properties of the substrate. The cases with yellow background and red text are from this work and previous work, as follows: PZT ($\Phi = 5.3 \text{ eV}$)/SRO ($\Phi = 4.9 \text{ eV}$) [8,24] PZT ($\Phi = 5.3 \text{ eV}$)/LSMO ($\Phi = 5.2 \text{ eV}$), inward polarization [24,39,51]; PbTiO₃/DyScO₃ with a similar work function, resulting polarization modulated [70]; BTO ($\Phi = 4.8 \text{ eV}$)/SRO ($\Phi = 4.9 \text{ eV}$), outward polarization [71]; PZT ($\Phi = 5.3 \text{ eV}$)/Pt ($\Phi = 5.65 \text{ eV}$), outward polarization [17].

the surface density of compensating charges $P \approx eN_{\text{def}}L$, L being the thickness of the film and e the elementary charge. The lower limit for the film thickness to still show ferroelectricity may then be written as

$$L > \frac{2\epsilon(T)\epsilon_{\text{def}}}{eP} \approx 3.2\text{--}7.9 \text{ nm}, \quad (3)$$

by use of the above values. This is close to the lower limit where an out-of-plane polarization is observed in our experiments, typically PZT/SRO/STO(001); nevertheless, even lower thickness (1.2–2.0 nm) in PbTiO₃/STO(001) films still showing ferroelectricity at room temperature has been reported [26,27].

(d) The interface field is computed in each semiconducting material by solving of the Poisson equation, where the inner potential is manifested by band bending: the minimum of the conduction band E_C , the maximum of the valence band E_V , and the donor or acceptor levels E_D or E_A will be affected by the inner potential for electrons $-e\phi(x)$, where $\phi(x)$ is the electrostatic potential. The Poisson equation containing, in order, contributions from electrons in the conduction band, negatively ionized acceptors, holes in the valence band, and positively ionized donors is written as

$$\frac{d^2\phi}{dx^2} = \frac{e}{\epsilon} \left\{ N_C F_{1/2} \left(\frac{E_F - E_C + e\phi}{k_B T} \right) + \frac{N_A}{1 + 2 \exp[(E_A - E_F - e\phi)/k_B T]} - N_V F_{1/2} \left(\frac{E_V - E_F - e\phi}{k_B T} \right) - \frac{N_D}{1 + 2 \exp[(E_F - E_D + e\phi)/k_B T]} \right\}, \quad (4)$$

where

$$F_{1/2}(x) = \frac{2}{\sqrt{\pi}} \int_0^\infty \frac{y^{1/2} dy}{1 + \exp(y-x)} \approx \begin{cases} e^x, & x < -2, \\ \frac{4}{3\sqrt{\pi}} x^{3/2}, & x > 5, \end{cases} \quad (5)$$

is the Fermi integral, and

$$N_{C,V} = \left(\frac{2\pi m_{e,h}^* k_B T}{h^2} \right)^{3/2}, \quad (6)$$

are densities of states in the conduction band and the valence band, respectively ($m_{e,h}^*$ are effective masses of electrons and holes, respectively, h is the Planck constant, k_B is the Boltzmann constant, T is the temperature). N_D and N_A are densities of donors and acceptors. Eq. (4) may be solved numerically and, in some cases, also analytically to yield the shape of the inner potential. However, for the next purposes of this study, which rely on the evaluation

of the interface field, a considerable simplification may be considered. Let us write Eq. (4) in a condensed way:

$$\frac{d^2\phi}{dx^2} = f(\phi(x)), \quad (7)$$

where f is a simple, integrable function [sum of exponentials or power-law functions, Eq. (5)]. By multiplying both sides by the derivative of the potential and integrating the expression from 0 to L , L being the thickness of the film, one obtains

$$\frac{d^2\phi}{dx^2} \cdot \frac{d\phi}{dx} = f(\phi(x)) \cdot \frac{d\phi}{dx}, \quad (8)$$

$$\left(\frac{d\phi}{dx} \right)_L^2 - \left(\frac{d\phi}{dx} \right)_0^2 = 2 \int_{\phi(0)}^{\phi(L)} f(\phi) d\phi = 2F(\phi(L)) - 2F(\phi(0)), \quad (9)$$

where F is the primitive function of f . Now, for all films investigated below we suppose that the electric field at the outer surface ($x=L$) vanishes (in the absence of the ferroelectric polarization), and we choose also the potential at the outer surface as a reference, such that $\phi(L)=0$, $(d\phi/dx)_L=0$. In these conditions, one obtains a simple expression for the electric field ε at the interface:

$$\left(\frac{d\phi}{dx} \right)_0^2 = \varepsilon^2(0) = 2F(\phi(0)) - 2F(0), \quad (10)$$

This is an immediate connection between the field at the origin and the potential drop on the sample $\phi(0)$.

(e) The next step is to evaluate the position of E_A and E_D in PZT and STON. According to Ref. [72], in PbTiO₃ there are two types of oxygen vacancies (donors), situated 0.06 and 0.3 eV below the conduction band. Also according to Ref. [72], lead vacancies implies an acceptor level quite close to E_V . We assume that in PZT with a Ti-to-Zr ratio of approximately 4:1 the situation is close to that of PbTiO₃. We also need to estimate the position of the Nb-donor-impurity level in STON. Here there were no available data in the literature; but if we use an excitonic model [73], the position of this level should be $m^*/(\epsilon_r^2 m_0)$ times the Rydberg energy (≈ 13.6 eV) below E_C . Owing to the large value of the dielectric constant in STO, $\epsilon_r \approx 300$ [57], the position of the Nb-donor-impurity level is also fairly close to E_C . Thus, the problem is simplified considerably, at least in a first approximation: Nb impurities in STON and oxygen vacancies in n -type PZT lie close to the minimum of the conduction band, while lead vacancies in p -type PZT lie close to the maximum of the valence band.

B. Interface between intrinsic PZT and STON

STON has a lower work function than PZT, and thus electrons migrate from STON to PZT, leaving a region of spatial charge formed by positively ionized donors. The Fermi level is close to E_C (or E_D) in the bulk of STON, and near the interface the bands are shifted upward, leaving most donors ionized. A similar situation occurs in the case of a p -doped material with a higher work function and acceptor level close to the maximum of the valence band, which transfers holes through the interface and remains with a sheet of negatively ionized acceptors. We write the solutions for both cases, knowing that for STON we must retain the n -type case. The Poisson equation has a simple solution:

$$\phi(x) = \pm \frac{eN_{A,D}}{2\epsilon}(x - x_0)^2, \quad (11)$$

for $x \leq x_0$, with the plus sign for acceptors and the minus sign for donors. For $x > x_0$, $\phi(x) = 0$. The depth of the depleted region may be immediately computed from the interface band bending:

$$x_0 = \left(\frac{2\epsilon|\phi(0)|}{eN_{A,D}} \right)^{1/2}, \quad (12)$$

The dependence of the electric field is obtained by derivation of Eq. (11):

$$\varepsilon(x) = \mp \frac{eN_{A,D}}{\epsilon}(x - x_0), \quad (13)$$

and the electric field at the origin (in this material) is written as

$$\varepsilon(0) = \pm \left(\frac{2N_{A,D}e|\phi(0)|}{\epsilon} \right)^{1/2}. \quad (14)$$

In an intrinsic semiconductor (PZT in this case) subject to charge injection, the Poisson equation is written as follows:

$$\frac{d^2\phi}{dx^2} = \frac{e}{\epsilon} \left[N_C \exp\left(\frac{E_F - E_C + e\phi}{k_B T}\right) - N_V \exp\left(\frac{E_V - E_F - e\phi}{k_B T}\right) \right] = \frac{2en_0}{\epsilon} \sinh\left(\frac{e\phi}{k_B T}\right), \quad (15)$$

where the carrier density of the intrinsic semiconductor n_0 is introduced. With the notation

$$v = \frac{e\phi}{k_B T}, \quad l_0 = \left(\frac{\epsilon k_B T}{e^2 n_0} \right)^{1/2}, \quad x' = \frac{x}{l_0}, \quad L' = \frac{L}{l_0}, \quad (16)$$

the Poisson equation becomes simply

$$\frac{d^2v}{dx'^2} = 2 \sinh v, \quad (17)$$

and the field at the origin is connected to the total potential drop on the film [Eq. (10)], which in this case becomes

$$\varepsilon(0) = \pm 2 \left[\frac{n_0 k_B T}{\epsilon} (\cosh v(0) - 1) \right]^{1/2}. \quad (18)$$

If STON (material 1, work function Φ_1) is interfaced with intrinsic PZT (material 2, work function Φ_2), the interface fields in these materials are written as

$$\varepsilon_1(0) = \left(\frac{2N_D k_B T}{\epsilon_1} \varphi_1 \right)^{1/2} = \left[\frac{2N_D k_B T}{\epsilon_1} (\varphi - \varphi_2) \right]^{1/2}, \quad (19)$$

$$\varepsilon_2(0) = 2 \left[\frac{n_0 k_B T}{\epsilon_2} (\cosh \varphi_2 - 1) \right]^{1/2}, \quad (20)$$

where φ_1 and φ_2 are potential-energy drops on both materials (in the unit of $k_B T$), $\varphi_1 + \varphi_2 = \varphi$, with

$$\varphi = \frac{\Phi_2 - \Phi_1}{k_B T}. \quad (21)$$

See Fig. 4. The electric displacement is continuous at the interface (or, equivalently, the system is neutral):

$$\epsilon_1 \varepsilon_1(0) = \epsilon_2 \varepsilon_2(0). \quad (22)$$

A transcendental equation for the potential-energy drop on PZT follows:

$$\frac{\epsilon_1 N_D}{2\epsilon_2 n_0} (\varphi - \varphi_2) = \cosh \varphi_2 - 1. \quad (23)$$

This equation is solved numerically for $\epsilon_{r,1} = 300$, $\epsilon_{r,2} = 150$, for different values of n_0 and N_D . Finally, the interface field in PZT may be evaluated as

$$\varepsilon_2(0) = \frac{(2N_D \epsilon_1 k_B T)^{1/2}}{\epsilon_2} (\varphi - \varphi_2)^{1/2}, \quad (24)$$

and the results are given in Fig. 5. We represent also the donor densities corresponding to the two Nb concentrations investigated in the previous section, and derive that the interface field in both cases exceeds the coercive field $(5-7) \times 10^7 \text{ V m}^{-1}$. Thus, it is reasonable to suppose that this interface field suffices to induce the polarization oriented from STON toward PZT (i.e., outward polarization) of the PZT film near the interface region. For lower doping levels, the interface field is simply not enough to induce outward polarization. The case of PZT interfaced with intrinsic STO is discussed in the next subsection.

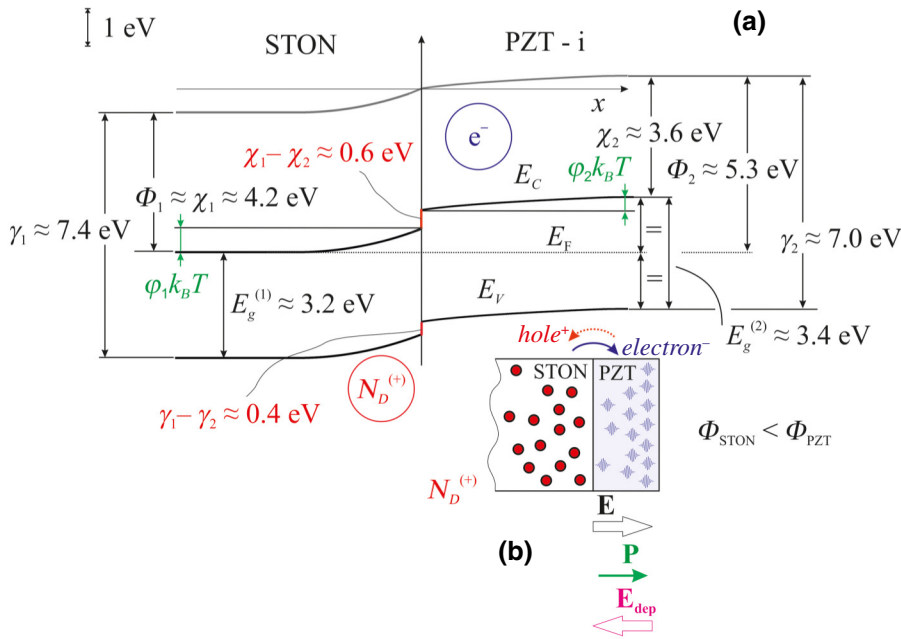


FIG. 4. (a) Band bending at the interface between STON and intrinsic (i) PZT. χ is the electron affinity, Φ is the work function, and γ is the ionization energy. (b) Charge distribution, interface fields, and setting of the polarization. Ionized impurities are represented as full circles, while mobile charge carriers are schematized as wave packets.

C. Interface between PZT and intrinsic STO

In this case, if intrinsic PZT is synthesized on intrinsic STO, no charge transfer will occur and the interface should be extremely abrupt. In practice, the synthesized material, which, in its intrinsic state, already has a work function higher than the work function of the substrate (5.3 eV versus 4.2 eV), undergoes a doping such as to allow charge transfer toward the substrate, yielding a smoothing of the energy bands. This is *p*-type doping, and even a consistent doping (the Pb content decreases by 14%, according to Table I). The first question to be analyzed is what is the work function of a (strongly) doped material with respect

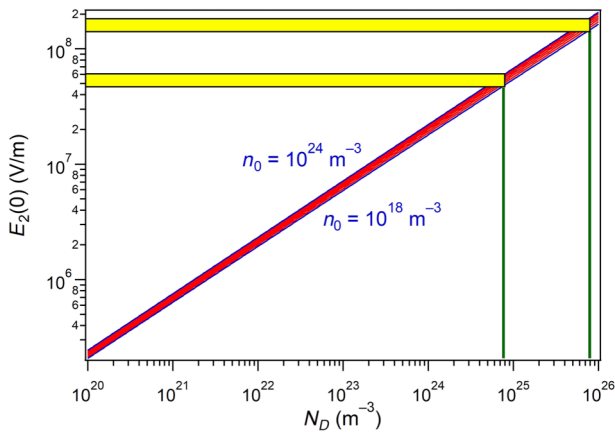


FIG. 5. The electric field in intrinsic PZT at the interface with STON as a function on the doping level in STON. The vertical green lines represent the two Nb doping levels investigated in this work. Solutions for different values of the carrier density in PZT (n_0) are concentrated in the narrow red region for $10^{18} \text{ m}^{-3} \leq n_0 \leq 10^{24} \text{ m}^{-3}$.

to that of the intrinsic material? Three different cases are outlined in Sec. S6 from the Supplemental Material [50]: (a) It could be that the work function of the doped materials is identical with that of the intrinsic material, and in this case the electron affinities vary considerably with doping. In this case *p-n* diodes would simply not work. (b) The opposite case is that of similar electron affinities, independent of doping, with the work function varying considerably from *n*-type doping to intrinsic material, then to *p*-type doping. (c) A more reasonable scenario is that neither of the above hypotheses is true, but the real situation lies somewhere in between: for example, the relative variations of work functions and affinities have opposite sign, $\Delta\Phi + \Delta\chi = 0$. This was confirmed, for example, for silicon, where large *n*- or *p*-type doping induces shifts in the work function (larger for *p*-type doping) of about one quarter of the band gap (0.3 eV) [74]. Note also that scenario (b) from Fig. S6, in the case of PZT, would imply a shift of half of the band gap, with a quite low work function (in the range of 3.6 eV) for heavily-*n*-doped material. Such a low work function for a common perovskite material would have drawn the attention of the thermionic emission community, but results are rather poor [75]. Hence, we start the evaluations regarding barriers and band bending between doped PZT and other materials by considering that the change in work function from heavily-*n*-doped to heavily-*p*-doped PZT is roughly half of the band gap; hence, if for the intrinsic material $\Phi_{\text{PZT}}^i \approx 5.3 \text{ eV}$, then $\Phi_{\text{PZT}}^n \approx 4.45 \text{ eV}$, and $\Phi_{\text{PZT}}^p \approx 6.15 \text{ eV}$.

Using the above value for *p*-type PZT, we schematize the band alignment between STO and *p*-doped PZT in Fig. 6(a). One may immediately see that there is a discontinuity in the valence band at the interface, and that

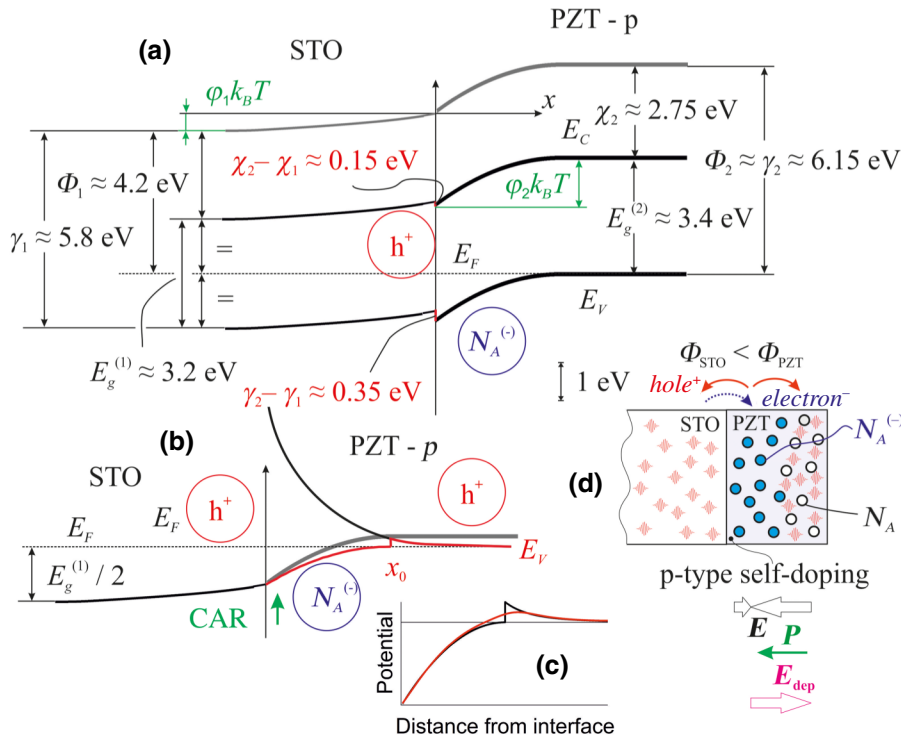


FIG. 6. Band alignment between STO and *p*-type PZT. (a) Band alignment obtained by use of a work function of 6.15 eV for *p*-type PZT and 4.2 eV for STO, together with the position of acceptors (Pb vacancies) close to the valence-band maximum in PZT. (b) Valence-band readjustment by taking into account the “common anion rule” (CAR). The bold gray curve represents the rigid shift of the previous valence band by the interface misfit energy $\gamma_2 - \gamma_1$. In this case, further from the interface, PZT becomes degenerate, and the Poisson equation in this region yields a decreasing potential energy from the interface (black curve). The real situation, represented by the red curve in (c) lies between the two previous cases. (d) Charge distribution, interface fields, and setting of the polarization. Ionized impurities are represented as full colored circles, neutral impurities are represented as empty circles, and mobile charge carriers are schematized as wave packets.

electrons are allowed to tunnel through this barrier. (Later we estimate the order of magnitude of the width of the depleted region to be in the range of a few nanometers; therefore, this “kink” region is considerably less extended.) An empirical rule introduced four decades ago [76,77], known as the “common anion rule,” assumes that the valence band should be adjusted such as to be continuous across the interface, since states building up valence bands have a similar origin, O $2p$ orbitals in this case. Thus, one expects in the zeroth approximation that the band alignment will be “readjusted” by a rigid shift toward higher energies in PZT so as to compensate the kink occurring at the interface in the valence band. This is schematized in Fig. 6(b) by the bold gray line. But, in this case, the Fermi energy will be placed inside the valence band, by an amount (0.4 eV) exceeding largely the thermal energy (0.025 eV). In this case, one has to investigate the Poisson equation in a degenerate semiconductor:

$$\begin{aligned} \frac{d^2 v}{dx^2} &= \frac{e^2 N_V}{\epsilon k_B T} [F_{1/2}(v) - F_{1/2}(v_0)] \\ &\approx \frac{4e^2 N_V}{3\sqrt{\pi} \epsilon k_B T} (v^{3/2} - v_0^{3/2}) = \frac{v^{3/2} - v_0^{3/2}}{l_V^2}, \end{aligned} \quad (25)$$

where

$$v(x) = \frac{E_V - E_F - e\phi(x)}{k_B T}, \quad v_0 = \frac{E_V - E_F}{k_B T}. \quad (26)$$

Approximating, as argued above, $v_0 \approx 0$, the solution has the form

$$v(x) = \frac{v(0)}{\left[1 + (v(0)^{1/4}/2\sqrt{5}l_V)x\right]^4}, \quad (27)$$

and the electric field for $x > x_0$ is given by

$$\begin{aligned} \varepsilon(x) &= -\frac{k_B T}{e l_V} \left[\frac{4}{5} v(x)^{5/2} - 2v_0^{3/2} v(x) \right]^{1/2} \\ &\approx -\frac{2k_B T}{e l_V \sqrt{5}} v(x)^{5/4}. \end{aligned} \quad (28)$$

In this case, relevant for the setting of the polarization in the outside region of the PZT film is the electric field at x_0 ; see Fig. 6(b). The potential energy here is approximately the offset $\Delta\gamma = \gamma_2 - \gamma_1$, the difference between the ionization energies of both materials. The total charge conservation of the heterostructure may be written as [(i) holes injected into STO] + [(ii) ionized acceptors in the depletion region $x < x_0$] + [(iii) holes injected in the degenerate region $x \geq x_0$] = 0. For (i) and (ii), we use the formalism developed in Sec. IVB; for (iii), we use Eq. (28) multiplied by the permittivity of PZT, and assume a vanishing field at the surface of PZT, in the absence of polarization. In total

[(i) + (iii)] = −(ii)

$$\begin{aligned} & 2(\epsilon_1 n_0 k_B T)^{1/2} (\cosh \varphi_1 - 1)^{1/2} \\ & + \frac{4}{\sqrt{15\sqrt{\pi}}} (\epsilon_2 N_V k_B T)^{1/2} \left(\frac{\Delta\gamma}{k_B T} \right)^{5/4} \\ & = [2\epsilon_2 N_A k_B T (\varphi - \varphi_1)]^{1/2}, \end{aligned} \quad (29)$$

where n_0 is the charge-carrier density in intrinsic STO, N_V is the density of states in the valence band in PZT, $\varphi k_B T$ is the difference between the work functions (known), see Eq. (21), and $\varphi_1 k_B T$ is the potential-energy drop on STO. φ_1 is derived from the above transcendental equation (it ranges from 25.67 for $n_0 = 10^{18} \text{ m}^{-3}$ to 12.11 for $n_0 = 10^{18} \text{ m}^{-3}$), N_V being estimated by use of the free-electron mass in Eq. (6) to be $2.4 \times 10^{25} \text{ m}^{-3}$, the dielectric constants being considered to be 150 and 300 for PZT and STO, respectively, and $N_A = 1.5625 \times 10^{27} \text{ m}^{-3}$, corresponding to 0.1 vacancies per formula unit. The thickness of the depleted region in PZT is derived as

$$x_0 = \left[\frac{2\epsilon_2 k_B T}{e^2 N_A} (\varphi - \varphi_1) \right]^{1/2}. \quad (30)$$

This yields 3.8–4.2 nm for the above input values; this is less than the thickness of the layer (10 nm); hence, the proposed model has no inconsistency from this point of view. The maximum electric field at the interface between the depleted region and the degenerate region of PZT is written as

$$\epsilon_2(x_0) = -\frac{4}{\sqrt{15\sqrt{\pi}}} \left(\frac{N_V k_B T}{\epsilon_2} \right)^{1/2} \left(\frac{\Delta\gamma}{k_B T} \right)^{5/4}, \quad (31)$$

and this is independent of the STO parameters (carrier density and dielectric constant). This yields $-1.8 \times 10^8 \text{ V m}^{-1}$, and its modulus greatly exceeds the coercive field, yielding inward polarization. By looking at the qualitative picture in Fig. 6(c), we see the maximum field will be a fraction (about 0.5) from the above computed value $\epsilon_2(x_0)$, but it will still be larger than the estimated coercive field, $5\text{--}7 \times 10^7 \text{ V m}^{-1}$. Hence, we think we offer a reasonable scenario for the realization of the inward polarization for PZT/STO.

D. Interface between PZT and SRO

SRO has a lower work function than PZT (4.8–4.9 eV). Thus, the first mechanism one may think about is charge injection (electrons) from SRO to PZT. Next, we consider that the metal reaction to this charge accumulation in the semiconductor is reasonably described by the formation of image charges inside it. In Fig. 7(a) this situation is schematized by our assuming an antisymmetric potential variation inside the semiconductor and in the metal.

In this case, electron excess in the semiconductor corresponds to electron deficit in the metal, manifested by the band bending of the bottom of the valence band, yielding a lower electron density near the interface with respect to the neutral metal. For the metal we assume that the Poisson equation (4) is not entirely correct, since for an ideal metal the dielectric constant is nearly infinity. A perfect metal would generate images of individual charges from the semiconductor, and thus also image dipoles of the polarized semiconductor, not taking into account the ferroelectric polarization, but just the polarizability effects [78]. Thus, in this ideal case the region of the metal near the interface may be viewed as an extension of the ionic semiconductor, through the introduction of these image charges; also the dielectric constant will be equal to that of the semiconductor. Thus, in the region of the metal we suppose that the charge density is antisymmetric with respect to the interface, the electric field is symmetric, and the potential, again, is antisymmetric.

In a more sophisticated model, one may introduce the Thomas-Fermi (TF) length, which takes into account the polarization of the free-electron gas:

$$\begin{aligned} r_{\text{TF}} &= \sqrt{\frac{\epsilon_0}{e^2 g(\epsilon_F)}} \times \\ & \left(= \sqrt{\frac{2\epsilon_0 \epsilon_F}{3e^2 n}} \text{ for the free-electron gas model} \right), \end{aligned} \quad (32)$$

where ϵ_F is the electron kinetic energy at the Fermi level, n the electron density, and $g(\epsilon)$ the density of states. For the formation of image charges, the TF screening length means the perturbation of the electron gas around a point charge, where the local potential behaves as a screened Coulomb potential, proportional to $\exp(-r/r_{\text{TF}})/r$. That is, well-localized charges are “blurred” by the electron gas on a spatial scale r_{TF} , which is below 1 Å for most metals (interesting diffraction-like phenomena may occur from simple electrostatics, but it is clear that on this scale quantum effects prevail). Anyway, for larger scales (above 1 Å) all considerations related to the formation of image charges are valid, especially since the Thomas-Fermi screening length is below the typical ionic radius of a ionized impurity and also less than interionic separations in the semiconductor material.

All these arguments suggest that it is sufficient to solve the Poisson equation in the semiconductor region by assuming that half of the total band bending $\varphi k_B T/2$ is the potential-energy drop in the semiconductor. Applying Eq. (18) for charge injected into an intrinsic semiconductor, we

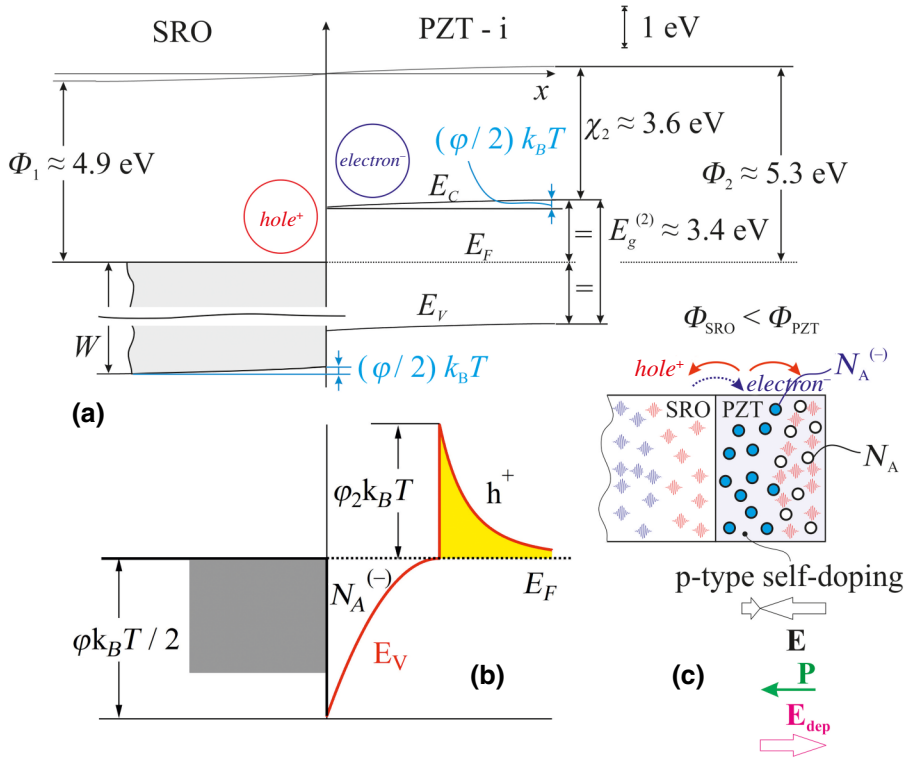


FIG. 7. Interface of SRO with PZT. (a) The case of an interface between intrinsic (i) PZT with a metal with a lower work function. Electrons are injected from the metal inside the semiconductor, leaving positive charge in the metal, which may be accounted for in an image-charge model. The band bending in PZT is half of the difference of the two work functions. (b) The case of *p*-type self-doping of PZT and hole promotion from PZT into SRO and toward the surface. (c) A scheme of the proposed mechanism, with the same color codes as in Fig. 5 and 6.

obtain

$$\begin{aligned} \varepsilon_2(0) &= 2 \left\{ \frac{n_0 k_B T}{\varepsilon_2} \left[\cosh \left(\frac{\varphi}{2} \right) - 1 \right] \right\}^{1/2} \\ &= 1.35 \times (10^5 - 10^8) \text{ V m}^{-1} \\ &\text{for } n_0 = (10^{18} - 10^{24}) \text{ m}^{-3}, \end{aligned} \quad (33)$$

where φ is the difference between work functions, in the unit of thermal energy $k_B T$ (about 16). In principle, for relatively high equilibrium charge density in PZT (10^{23} – 10^{24} m^{-3}), the electric field, oriented outward, would be sufficient to polarize the ferroelectric in this direction.

Obviously, this is not the case in the present study, nor was it in previous studies with ferroelectrics on metals with a lower work function [8,24,49]. Moreover, the fact that in the case of interfaces with a metal with a higher work function (Pt), the polarization is oriented outward [17,65] reinforces the hypothesis of a mechanism driven by the near-interface field. From the above analysis, a reasonable supposition is that the charge-carrier density inside (intrinsic) PZT is lower than about 10^{23} m^{-3} and, if some other interface effect might occur to promote a stable polarization, the heterostructure follows this route. In the following we detail also other arguments against this scenario, although just the experimental facts should suffice.

From the XPS analysis (Table I) we derive that in this case *p*-type self-doping by creation of Pb vacancies is

even stronger than in the case of the PZT/STO interface (more than 0.2 Pb vacancies per formula unit). If such doping occurs, then holes will be injected into the metal, leaving a sheet of ionized acceptors near the interface. For a band bending of about 0.675 eV inside PZT (taking into account that we suppose a work function of 6.15 eV for *p*-doped PZT) and $N_V \approx 1.5625 \times 10^{27} \text{ m}^{-3}$, corresponding to 0.1 Pb vacancies per formula unit (unit cell), we obtain using Eq. (14) a quite large interface field of about $5.1 \times 10^8 \text{ V m}^{-1}$, oriented outward. This would largely suffice to promote outward polarization but, again, this is not confirmed experimentally. Thus, we must supplement this hypothesis by considering, as in the case of the interface with STO, that in some region near the interface ionized acceptors prevail, but toward the surface of PZT, the semiconductor is degenerate and the potential energy decreases toward the surface, yielding a field oriented inward. This is schematized in Fig. 7(b).

In this model, there is no *a priori* hypothesis helping one to derive the delimitation between the depleted region and the region of degenerate semiconductor (i.e., x_0) nor the potential energy at this point. In the case of the interface with STO, we use the (empirical) common anion rule and stipulate that $V(x_0) = -e\Phi(x_0) \approx \gamma_2 - \gamma_1$, the difference between ionization energies. In this case, an additional hypothesis would be that the *overall PZT film is neutral* (i.e., the negative charge of ionized acceptors from the depletion region is compensated by the positive charge of holes promoted toward the surface). By using the corresponding terms, Eq. (29), dropping the first term, which

corresponds to holes injected into STO, and assuming that the potential-energy drop on PZT is half of the difference between work functions, the neutrality condition implies

$$\frac{4}{\sqrt{15\sqrt{\pi}}}(\epsilon_2 N_V k_B T)^{1/2} \varphi_2^{5/4} = (\epsilon_2 N_A k_B T \varphi)^{1/2}, \quad (34)$$

where φ_2 is the potential energy in x_0 in the unit of $k_B T$ [see Fig. 7(b)],

$$\varphi_2 = \left(\frac{15\sqrt{\pi} N_A}{16 N_V} \varphi \right)^{2/5} \approx 24.25, \quad (35)$$

which corresponds to about 0.6 eV. The delimitation between the depleted region and the degenerate region is estimated as

$$x_0 = \left(\frac{\epsilon_2 k_B T \varphi_2}{e^2 N_A} \right)^{1/2} \approx 1.8 \text{ nm}. \quad (36)$$

Finally, the inward-oriented electric field is estimated as [similarly to Eq. (31)]

$$\begin{aligned} \varepsilon_2(x_0) &= -\frac{4}{\sqrt{15\sqrt{\pi}}} \left(\frac{N_V k_B T}{\epsilon_2} \right)^{1/2} \varphi_2^{5/4} \\ &\approx -2.9 \times 10^9 \text{ V m}^{-1}. \end{aligned} \quad (37)$$

According to Fig. 7(c), an inward-oriented field of some 10^9 V m^{-1} may be still stipulated, still large enough to drive the polarization in its direction.

This is clearly larger in modulus than the interface fields produced either by electron injection from SRO toward intrinsic PZT (up to $1.35 \times 10^8 \text{ V m}^{-1}$) or by the formation of a depleted layer with negatively ionized acceptors (up to $5.1 \times 10^8 \text{ V m}^{-1}$). It looks as if when self-doping occurs this produces from the beginning a large number of holes so as to cause the part of the film that is not depleted directly to have degenerate character and, eventually, to induce inward polarization. The same exercise may be performed with considerably lower values of φ . Even with $\varphi = 1$ (i.e., a drop of the potential energy on PZT equal to the thermal energy), one obtains from Eq. (35) φ_2 about 6.5 times the thermal energy, $x_0 \approx 0.9 \text{ nm}$, and an inward-oriented field at x_0 of about $5.1 \times 10^8 \text{ V m}^{-1}$. Thus, one argument for establishing such an unusual situation in semiconductor physics (a depleted and a degenerate region coexisting in the same film) is that this results in the easiest establishment of a state with lower energy, which is the ferroelectric state. But there might also be fundamental arguments regarding the need to have electrical neutrality in separated dielectric or semiconducting parts of the heterostructure, irrespective of the use of the image-charge model that would compensate charge accumulated in PZT.

Similar arguments may now be applied, reversed, to explain the outward polarization when the ferroelectric film is interfaced with a metal with a higher work function. In this case, n -type self-doping is expected to occur (creation of oxygen vacancies), and the bare material is again nearly degenerate, although there are some oxygen-vacancy levels deeper in the band gap, $E_C - E_D \approx 0.06$ and 0.3 eV; it is, however, reasonable to take into account mostly the former ones. Near the interface with the metal, a depleted region with positively ionized donors is built up, followed by a degenerate n -type region for the remaining part of the film, toward the surface.

Note also that this scenario provides charge carriers and their opposite-sign counterparts (ionized impurities) to build up the compensating-charge layers, once the polarization is set. Although in the first hypothesis (electron injection from SRO into intrinsic PZT) also electrons are found in PZT, there is no positive-charge counterpart in the material; the only positive-charge counterparts are image charges in the metal, a hypothesis which is somehow questionable. In the second hypothesis, with the formation of only a depleted negative layer near the interface, there is no other charge that would compensate the depolarization field, toward the surface of the film. The amount of charge that may be used for compensation may be estimated from Eq. (37), assuming that the electric field without ferroelectricity vanishes at the surface, and with multiplication by the dielectric constant. This yields 1.3 cm^{-2} for a field of 10^9 V m^{-1} . Undoubtedly, once the polarization is set, new electrostatics is involved that could promote larger amounts of charge transfer from the substrate, but only this evaluation yields a sufficient surface charge density to compensate the strong polarization in PZT of about $0.6\text{--}1 \text{ cm}^{-2}$.

One last consideration concerns the presence of contamination layers. From PFM (see Sec. S2 from the Supplemental Material [50]) and also XPS of “dirty” films (see Sec. S4 from the Supplemental Material [50]), especially after annealing in UHV, when traces of carbon are still present on the surface (see Sec. S5 from the Supplemental Material [50]), one may derive that the outward polarization is present on these contaminated surfaces. That the binding energies from the surface are rather close to a state with no out-of-plane polarization for the as-introduced samples, according to Figs. S4(a₄)–(d₄), may be interpreted by a model such as that presented in Fig. 1(b); the core levels from the substrate are close to a “neutral” (or $P^{(0)}$) state, but the C 1s binding energy from the adventitious contamination is lower than the accepted value (284.3 eV versus 284.6–285 eV). This reveals, again, an outward ($P^{(+)}$) polarization state in the presence of contaminants. The composition of the as-introduced sample, by not taking into account O 1s levels with binding energy larger than 531 eV, which are attributed to contaminants [79], may be written as 0.35 PbO plus $\text{PbZr}_{0.23}\text{Ti}_{0.77}\text{O}_{2.94}$.

It is reasonable to find some PbO on the surface, since the PLD target is a PZT ceramic enriched in lead oxide. On the other hand, if the surface is disordered, photoelectron-diffraction and electron-mean-free-path effects are smeared out. In conclusion, with the exception of excess PbO, the as-introduced sample is nearly stoichiometric, with a slight oxygen deficit (i.e., one can reasonably suppose that it is n doped and, according to the considerations from Sec. IVC, that its work function is lower than 5.3 eV). Its work function might be even lower than the work function of the substrate. In this case (presence of contaminants), the film undergoes n -type self-doping, and all the considerations from this subsection are still valid, especially the formation of a depleted layer near the interface this time consisting of positively ionized donors, with an outer degenerate n -type region, toward the surface. This will promote a field oriented outward in PZT to impose this kind of polarization. Moreover, during the synthesis, the film will undergo n -type self-doping with the formation of oxygen vacancies. This is exactly the result discussed in Ref. [8]. Similar outward polarization was reported for ultrathin PbTiO₃ films on STO [27,28], however by a method (metal-oxide chemical vapor deposition), which did not allow the absence of contaminants [80]. When PZT is synthesized on LSMO, measurements in the presence of contaminants yield outward polarization [81], while for ultraclean systems the inward polarization is stabilized (see Fig. 3) [24,51]. All these data reinforce the belief that organic contaminants [15] may act as donors, promoting the n -type character of the film. If such a film is heated in an oxygen atmosphere, carbon contamination will be consumed, oxygen vacancies will be filled in, and one obtains the intrinsic material with a work function higher than that of the metal substrate. With further annealing, the PZT will release Pb to achieve p -type self-doping and allow this time an inward-oriented polarization. However, this is a simplified picture, and the influence of contaminant molecules in controlling self-doping, interface fields, and polarization deserves a more extended correlated theoretical and experimental investigation.

V. CONCLUSION

The orientation of the out-of-plane polarization of a ferroelectric thin film clearly depends on the substrate used, as revealed by XPS. The difference between the work functions of the ferroelectric and the substrate implies that charge transfer occurs at the interface, and the ferroelectric undergoes a self-doping so as to generate the necessary charges. The main ingredient of the interpretation is the ability of the interface field developed between the substrate and the initially unpoled ferroelectric to set the orientation of the polarization (i.e., to exceed the coercive field). The easiest case to explain is that of a ferroelectric synthesized on a doped semiconductor, more specifically on an

n -doped semiconductor with a lower work function or on a p -doped semiconductor with a higher work function. An interface field is created between ionized impurities from the depleted region in the semiconducting substrate and charge injected into the intrinsic ferroelectric. This field drives a polarization oriented from the substrate to the ferroelectric film for the first case (n -doped substrate) and in the opposed direction for the second case. The model we propose is able to estimate a lower substrate doping limit, below which the interface field is lower than the coercive field and therefore cannot set the orientation of the polarization.

When the ferroelectric is synthesized on an insulator with a lower work function [STO(001)], the ferroelectric needs holes to be transferred, and will progressively contain negatively ionized acceptors near the interface. The doping level being elevated, together with considerations on the continuity of the valence band (“common anion rule”) yields the setup of a degenerate region in the ferroelectric material toward the surface. The field, which further induces polarization, is formed between the depleted region with ionized acceptors and the outer region with excess holes, pointing toward the substrate.

The most difficult explanation is for the synthesis of a ferroelectric film on a metal with different work functions. For a metal with a lower work function, qualitative arguments are brought against a mechanism that would promote electrons from the metal inside the ferroelectric semiconductor; this should yield an interface field oriented outward. Instead, a mechanism similar to the case of an insulating substrate with a lower work function may be proposed also in this case, and the metal itself is regarded just as a “mirror” for charges formed in a semiconductor. For these heterostructures, an essential role is played also by the availability of charges of opposite signs at the extremities of the ferroelectric semiconductor, which afterward will compensate the depolarization field. Anyway, this mechanism, reversed by use of electrons instead of holes and n -type self-doping instead of p -type self-doping, might explain the outward polarization when metal substrates with a higher work function are used. Finally, we give an explanation also of the possible mechanisms inducing outward polarization for PZT/SRO in the presence of contaminants, but a complete explanation should contain more details of the surface chemistry of these structures.

Finally, the actual simplified model does not preclude fine effects related to interface terminations [25,41,42]. Most probably these latter effects will prevail when the interfaces are engineered at the single-atomic-layer level. But, for less-defined interfaces where such fine effects are mediated, a charge-transfer and electrostatic model might be easier to tackle than detailed *ab initio* calculations. More-complicated heterostructures and other interesting phenomena, such as the influence of a ferroelectric gate on a conduction channel and, in some cases, on

its metal-to-insulator transitions [82,83], are expected to be modeled starting with the formalism presented in this work, applied to heterostructures of increased complexity. For example, in the case of insufficient interface polarization field $\varepsilon(x_0)$, one expects the formation of domains, but a complete theory of domain formation related to depolarization and interface electrostatics is still expected to be formulated.

ACKNOWLEDGMENTS

This work was funded by the Romanian Ministry for Research and Innovation through the National Institute of Materials Physics (NIMP) Core Program PN18-11/2018, and by UEFISCDI through project PN-III-P1-1.2-PCCDI-2017-0152 (Grant No. 75PCCDI/2018). N.G.A. acknowledges funding from the postdoctoral UEFISCDI project PN-III-P1-1.1-PD-2016-1322.

-
- [1] J. F. Scott, *Ferroelectric Memories* (Springer, Heidelberg, 2000).
- [2] K. Uchino, *Ferroelectric Devices* (Marcel Dekker, New York, 2000).
- [3] R. V. Wang, D. D. Fong, F. Jiang, M. J. Highland, P. H. Fuoss, C. Thompson, A. M. Kolpak, J. A. Eastman, S. K. Streiffer, A. M. Rappe, and G. B. Stephenson, Reversible Chemical Switching of a Ferroelectric Film, *Phys. Rev. Lett.* **102**, 047601 (2009).
- [4] S. Ghosh, U. Chowdhury, S. Roy, and R. Bandyopadhyay, Detection of low ppm carbon monoxide with charge ordered LuFe_2O_4 gas sensor – A novel sensing mechanism, *Ceram. Int.* **42**, 14944 (2016).
- [5] K. Garrity, A. M. Kolpak, S. Ismail-Beigi, and E. I. Altman, Chemistry of ferroelectric surfaces, *Adv. Mater.* **22**, 2969 (2010).
- [6] C. Y. Chao, Z. H. Ren, Y. H. Zhu, Z. Xiao, Z. Liu, G. Xu, J. Q. Mai, X. Li, G. Shen, and G. R. Han, Self-templated synthesis of single-crystal and single-domain ferroelectric nanoplates, *Angew. Chem. Int. Ed.* **51**, 9283 (2012).
- [7] A. Kakekhani, S. Ismail-Beigi, and E. I. Altman, Ferroelectrics: A pathway to switchable surface chemistry and catalysis, *Surf. Sci.* **650**, 302 (2016).
- [8] L. C. Tănase, N. G. Apostol, L. E. Abramiuc, C. A. Tache, L. Hrib, L. Trupinã, L. Pintilie, and C. M. Teodorescu, Ferroelectric triggering of carbon monoxide adsorption on lead zirconate-titanate (001) surfaces, *Sci. Rep.* **6**, 35301 (2016).
- [9] B. O. Alawode and A. M. Kolpak, $\text{PbTiO}_3(001)$ capped with $\text{ZnO}(11\bar{2}0)$: an ab initio study of effect of substrate polarization on interface composition and CO_2 dissociation, *J. Phys. Chem. Lett.* **7**, 1310 (2016).
- [10] L. Li, P. A. Salvador, and G. S. Rohrer, Photocatalysts with internal electric fields, *Nanoscale* **6**, 24 (2014).
- [11] M. A. Khan, M. A. Nadeem, and H. Idriss, Ferroelectric polarization effect on surface chemistry and photo-catalytic activity: A review, *Surf. Sci. Rep.* **71**, 1 (2016).
- [12] Y. G. Yuan, Z. G. Xiao, B. Yang, and J. S. Huang, Arising applications of ferroelectric materials in photovoltaic devices, *J. Mater. Chem. A* **2**, 6027 (2014).
- [13] Y. F. Cui, J. Briscoe, and S. Dunn, Effect of ferroelectricity on solar-light-driven photocatalytic activity of BaTiO_3 – influence on the carrier separation and stern layer formation, *Chem. Mater.* **25**, 4215 (2013).
- [14] Z. Z. Zhang, P. Sharma, C. N. Borca, P. A. Dowben, and A. Gruverman, Polarization-specific adsorption of organic molecules on ferroelectric LiNbO_3 surfaces, *Appl. Phys. Lett.* **97**, 243702 (2010).
- [15] L. E. Ștoflea, N. G. Apostol, L. Trupinã, and C. M. Teodorescu, Selective adsorption of contaminants on $\text{Pb}(\text{Zr,Ti})\text{O}_3$ surfaces shown by X-ray photoelectron spectroscopy, *J. Mater. Chem. A* **2**, 14386 (2014).
- [16] A. Rajapitamahuni, J. Hoffman, C. H. Ahn, and X. Hong, Examining graphene field effect sensors for ferroelectric thin film studies, *Nano Lett.* **13**, 4374 (2013).
- [17] N. G. Apostol, G. A. Lungu, I. C. Bucur, C. A. Tache, L. Hrib, L. Pintilie, D. Macovei, and C. M. Teodorescu, Non-interacting, sp^2 hybridized carbon layers on ferroelectric lead zirconate-titanate, *RSC Adv.* **6**, 67883 (2016).
- [18] I. Pintilie, C. M. Teodorescu, C. Ghica, C. Chirila, A. G. Boni, L. Hrib, I. Pasuk, R. Negrea, N. G. Apostol, and L. Pintilie, Polarization-control of the potential barrier at the electrode interfaces in epitaxial ferroelectric thin films, *ACS Appl. Mater. Interfaces* **6**, 2929 (2014).
- [19] L. Pintilie, C. Ghica, C. M. Teodorescu, I. Pintilie, C. Chirila, I. Pasuk, L. Trupina, L. Hrib, A. G. Boni, N. G. Apostol, L. E. Abramiuc, R. Negrea, M. Stefan, and D. Ghica, Polarization induced self-doping in epitaxial $\text{Pb}(\text{Zr}_{0.20}\text{Ti}_{0.80})\text{O}_3$ thin films, *Sci. Rep.* **5**, 14974 (2015).
- [20] L. Pintilie and M. Alexe, Metal-ferroelectric-metal heterostructures with Schottky contacts. I. Influence of the ferroelectric properties, *J. Appl. Phys.* **98**, 124103 (2005).
- [21] L. Pintilie, I. Boerasu, M. J. M. Gomes, T. Zhao, R. Ramesh, and M. Alexe, Metal-ferroelectric-metal structures with Schottky contacts. II. Analysis of the experimental current-voltage and capacitance-voltage characteristics of $\text{Pb}(\text{Zr,Ti})\text{O}_3$ thin films, *J. Appl. Phys.* **98**, 124104 (2005).
- [22] P. X. Miao, Y. G. Zhao, N. N. Luo, D. Y. Zhao, A. T. Chen, Z. Sun, M. Q. Guo, M. H. Zhu, H. Y. Zhang, and Q. Li, Ferroelectricity and self-polarization in ultrathin relaxor ferroelectric films, *Sci. Rep.* **6**, 19965 (2016).
- [23] I. Pintilie, L. Trinca, L. Trupina, I. Pasuk, and L. Pintilie, Relation between domain structure and pyroelectric response in as-grown epitaxial $\text{Pb}(\text{Zr}_{0.2}\text{Ti}_{0.8})\text{O}_3$ thin films on substrates with different resistivity, *Mater. Res. Bull.* **93**, 201 (2017).
- [24] P. Maksymovych, S. Jesse, P. Yu, R. Ramesh, A. P. Bad-dorf, and S. V. Kalinin, Polarization control of electron tunneling into ferroelectric surfaces, *Science* **324**, 1421 (2009).
- [25] P. Yu, W. Luo, D. Yi, J. X. Zhang, M. D. Rossell, C.-H. Yang, L. You, G. Singh-Bhalla, S. Y. Yang, Q. He, Q. M. Ramasse, R. Erni, L. W. Martin, Y. H. Chu, S. T. Pantelides, S. J. Pennycook, and R. Ramesh, Interface control of bulk ferroelectric polarization, *Proc. Natl. Acad. Sci. U.S.A.* **109**, 9710 (2012).
- [26] D. D. Fong, G. B. Stephenson, S. K. Streiffer, J. A. Eastman, O. Auciello, P. H. Fuoss, and C. Thompson, Ferroelectricity in ultrathin perovskite films, *Science* **304**, 1650 (2004).
- [27] D. D. Fong, C. Cionca, Y. Yacoby, G. B. Stephenson, J. A. Eastman, P. H. Fuoss, S. K. Streiffer, C. Thompson,

- R. Clarke, R. Pindak, and E. A. Stern, Direct structural determination in ultrathin ferroelectric films by analysis of synchrotron x-ray scattering measurements, *Phys. Rev. B* **71**, 144112 (2005).
- [28] D. D. Fong, A. M. Kolpak, J. A. Eastman, S. K. Streiffer, P. H. Fuoss, G. B. Stephenson, C. Thompson, D. M. Kim, K. J. Choi, C. B. Eom, I. Grinberg, and A. M. Rappe, Stabilization of Monodomain Polarization in Ultrathin PbTiO₃ Films, *Phys. Rev. Lett* **96**, 127601 (2006).
- [29] N. G. Apostol, L. E. Stoflea, G. A. Lungu, C. A. Tache, L. Pintilie, and C. M. Teodorescu, Band bending at free Pb(Zr,Ti)O₃ surfaces analyzed by X-ray photoelectron spectroscopy, *Mater. Sci. Eng. B* **178**, 1317 (2013).
- [30] D. G. Popescu, M. A. Huşanu, L. Trupină, L. Hrib, L. Pintilie, A. Barinov, S. Lizzit, P. Lacovig, and C. M. Teodorescu, Spectro-microscopic photoemission evidence of charge uncompensated areas in Pb(Zr,Ti)O₃(001) layers, *Phys. Chem. Chem. Phys.* **17**, 509 (2015).
- [31] M. A. Huşanu, D. G. Popescu, C. A. Tache, N. G. Apostol, A. Barinov, S. Lizzit, P. Lacovig, and C. M. Teodorescu, Photoelectron spectroscopy and spectro-microscopy of Pb(Zr,Ti)O₃(111) thin layers: imaging ferroelectric domains with binding energy contrast, *Appl. Surf. Sci.* **352**, 73 (2015).
- [32] L. E. Abramiuc, L. C. Tănase, A. Barinov, N. G. Apostol, C. Chirilă, L. Trupină, L. Pintilie, and C. M. Teodorescu, Polarization landscape effects in soft X-ray-induced surface chemical decomposition of lead zirconate-titanate, evidenced by photoelectron spectromicroscopy, *Nanoscale* **9**, 11055 (2017).
- [33] F. Chen and A. Klein, Polarization dependence of Schottky barrier heights at interfaces of ferroelectrics determined by photoelectron spectroscopy, *Phys. Rev. B* **86**, 094105 (2012).
- [34] N. G. Apostol, L. E. Stoflea, G. A. Lungu, C. Chirila, L. Trupina, R. F. Negrea, C. Ghica, L. Pintilie, and C. M. Teodorescu, Charge transfer and band bending at Au/Pb(Zr,Ti)O₃ interfaces investigated by photoelectron spectroscopy, *Appl. Surf. Sci.* **273**, 415 (2013).
- [35] N. G. Apostol, L. E. Stoflea, G. A. Lungu, L. C. Tanase, C. Chirila, L. Frunza, L. Pintilie, and C. M. Teodorescu, Band bending in Au/Pb(Zr,Ti)O₃ investigated by X-ray photoelectron spectroscopy: Dependence on the initial state of the film, *Thin Solid Films* **545**, 13 (2013).
- [36] L. E. Stoflea, N. G. Apostol, C. Chirila, L. Trupina, R. Negrea, L. Pintilie, and C. M. Teodorescu, Schottky barrier versus surface ferroelectric depolarization at Cu/Pb(Zr,Ti)O₃ interfaces, *J. Mater. Sci.* **49**, 3337 (2014).
- [37] N. G. Apostol, L. E. Stoflea, L. C. Tănase, I. C. Bucur, C. Chirilă, R. F. Negrea, and C. M. Teodorescu, Band bending at copper and gold interfaces with ferroelectric Pb(Zr,Ti)O₃ investigated by photoelectron spectroscopy, *Appl. Surf. Sci.* **354**, 459 (2015).
- [38] I. C. Bucur, L. C. Tănase, L. E. Abramiuc, G. A. Lungu, C. Chirilă, L. Trupină, N. G. Apostol, R. M. Costescu, L. Pintilie, and C. M. Teodorescu, Triggering surface ferroelectric order in Pb(Zr,Ti)O₃(001) by deposition of platinum, *Appl. Surf. Sci.* **432**, 27 (2018).
- [39] C.-L. Wu, P.-W. Lee, Y.-C. Chen, L.-Y. Chang, C.-H. Chen, C.-W. Liang, P. Yu, Q. He, R. Ramesh, and Y.-H. Chu, Direct spectroscopic evidence of charge reversal at the Pb(Zr_{0.2}Ti_{0.8})O₃/La_{0.7}Sr_{0.3}MnO₃ heterointerface, *Phys. Rev. B* **83**, 020103(R) (2011).
- [40] J. M. Rondinelli and N. A. Spaldin, Structure and properties of functional oxide thin films: Insights from electronic-structure calculations, *Adv. Mater.* **23**, 3363 (2011).
- [41] H. Lu, X. Liu, J. D. Burton, C.-W. Bark, Y. Wang, Y. Zhang, D. J. Kim, A. Stamm, P. Lukashev, D. A. Felker, C. M. Folkman, P. Gao, M. S. Rzechowski, X. Q. Pan, C.-B. Eom, E. Y. Tsymlal, and A. Gruverman, Enhancement of ferroelectric polarization stability by interface engineering, *Adv. Mater.* **24**, 1209 (2012).
- [42] X. H. Liu, Y. Wang, P. V. Lukashev, J. D. Burton, and E. Y. Tsymlal, Interface dipole effect on thin film ferroelectric stability: First-principles and phenomenological modeling, *Phys. Rev. B* **85**, 125407 (2012).
- [43] G. Gerra, A. K. Tagantsev, N. Setter, and K. Parlinski, Ionic Polarizability of Conductive Metal Oxides and Critical Thickness for Ferroelectricity in BaTiO₃, *Phys. Rev. Lett.* **96**, 107603 (2006).
- [44] A. S. Karapuzha, N. K. James, H. Khanbareh, S. Van der Zwaag, and W. A. Groen, Structure, dielectric and piezoelectric properties of donor doped PZT ceramics across the phase diagram, *Ferroelectrics* **504**, 160 (2016).
- [45] J. E. Rault, G. Agnus, T. Maroutian, V. Pillard, P. Lecoeur, G. Niu, B. Vilquin, M. G. Silly, A. Bendounan, F. Sirotti, and N. Barrett, Interface electronic structure in a metal/ferroelectric heterostructure under applied bias, *Phys. Rev. B* **87**, 155146 (2013).
- [46] A. Zenkevich, M. Minnekaev, Y. Matveyev, Y. Lebedinskii, K. Bulakh, A. Chouprik, A. Baturin, K. Maksimova, S. Thiess, and W. Drube, Electronic band alignment and electron transport in Cr/BaTiO₃/Pt ferroelectric tunnel junctions, *Appl. Phys. Lett.* **102**, 062907 (2013).
- [47] L. M. Hrib, A. G. Boni, C. Chirila, I. Pasuk, I. Pintilie, and L. Pintilie, Electrode interface control of the Schottky diode-like behavior in epitaxial Pb(Zr_{0.2}Ti_{0.8})O₃ thin films: A critical analysis, *J. Appl. Phys.* **113**, 214108 (2013).
- [48] F. Chen, R. Schafranek, A. Wachau, S. Zhukov, J. Glaum, T. Granzow, H. von Seggern, and A. Klein, Barrier heights, polarization switching, and electrical fatigue in Pb(Zr,Ti)O₃ ceramics with different electrodes, *J. Appl. Phys.* **108**, 104106 (2010).
- [49] I. Krug, N. Barrett, A. Petraru, A. Locatelli, T. O. Montes, M. A. Niño, K. Rahmanizadeh, G. Bihlmayer, and C. M. Schneider, Extrinsic screening of ferroelectric domains in Pb(Zr_{0.48}Ti_{0.52})O₃, *Appl. Phys. Lett.* **97**, 222903 (2010).
- [50] See Supplemental Material at <https://link.aps.org/supplemental/10.1103/PhysRevApplied.10.034020> for S1 X-ray diffraction, S2 AFM and PFM, S3 LEED, S4 complete core-level XPS at several stages of sample preparation, S5 carbon 1s XPS spectra, and S6 possible variations of work functions (Φ) and electron affinities (χ) with doping.
- [51] C. M. Teodorescu, L. Pintilie, N. G. Apostol, R. M. Costescu, G. A. Lungu, L. Hrib, L. Trupină, L. C. Tănase, I. C. Bucur, and A. E. Bocîrneu, Low energy electron diffraction from ferroelectric surfaces. Dead layers and surface dipoles in ultraclean Pb(Zr,Ti)O₃(001), *Phys. Rev. B* **96**, 115438 (2017).

- [52] J. J. Yeh and I. Lindau, Atomic subshell photoionization cross sections and asymmetry parameters: $1 \leq Z \leq 103$, *At. Data Nucl. Data Tables* **32**, 1 (1985).
- [53] C. M. Teodorescu, J. M. Esteva, R. C. Karnatak, and A. El Afif, An approximation of the Voigt I profile for the fitting of experimental x-ray absorption data, *Nucl. Instrum. Methods Phys. Res. Sect. A – Accel. Spectrom. Dect. Assoc. Equip.* **345**, 141 (1994).
- [54] D. Mardare, D. Luca, C. M. Teodorescu, and D. Macovei, On the hydrophilicity of nitrogen-doped TiO₂ thin films, *Surf. Sci.* **601**, 4515 (2007).
- [55] P. Ghosez, J.-P. Michenaud, and X. Gonze, Dynamical atomic charges: The case of ABO₃ compounds, *Phys. Rev. B* **58**, 6224 (1998).
- [56] H. S. Lee, Y. S. Kang, S.-J. Cho, B. Xiao, H. Morkoç, T. D. Kang, G. S. Lee, J. B. Li, S.-H. Wei, P. G. Snyder, and J. T. Evans, Dielectric functions and electronic band structure of lead zirconate titanate thin films, *J. Appl. Phys.* **98**, 094108 (2005).
- [57] K. van Benthem, C. Elsässer, and R. H. French, Bulk electronic structure of SrTiO₃: Experiment and theory, *J. Appl. Phys.* **90**, 6156 (2001).
- [58] R. C. Neville, B. Hoeneisen, and C. A. Mead, Permittivity of strontium titanate, *J. Appl. Phys.* **43**, 2124 (1972).
- [59] M. Stengel and N. A. Spaldin, Origin of the dielectric dead layer in nanoscale capacitors, *Nature* **443**, 679 (2006).
- [60] L.-W. Chang, M. Alexe, J. F. Scott, and J. M. Gregg, Settling the “dead layer” debate in nanoscale capacitors, *Adv. Mater.* **21**, 4911 (2009).
- [61] J. A. Sanjurjo, E. López-Cruz, and G. Burns, High-pressure Raman study of zone-center phonons in PbTiO₃, *Phys. Rev. B* **28**, 7260 (1983).
- [62] L. Pintilie, I. Vrejoiu, D. Hesse, G. LeRhun, and M. Alexe, Extrinsic contributions to the apparent thickness dependence of the dielectric constant in epitaxial Pb(Zr,Ti)O₃ thin films, *Phys. Rev. B* **75**, 224113 (2007).
- [63] A. V. Dixit, N. R. Rajopadhye, and S. V. Boraskar, Secondary electron emission of doped PZT ceramics, *J. Mater. Sci.* **21**, 2798 (1986).
- [64] C. Yoshida, A. Yoshida, and H. Tamura, Nanoscale conduction modulation in Au/Pb(Zr,Ti)O₃/SrRuO₃ heterostructure, *Appl. Phys. Lett.* **75**, 1449 (1999).
- [65] J. F. Scott, K. Watanabe, J. Hartmann, and R. N. Lamb, Evolution of polarization and space charges in semiconducting ferroelectrics, *Ferroelectrics* **225**, 83 (1999).
- [66] P. Gao, C. T. Nelson, J. R. Jokisaari, S.-H. Baek, C. W. Bark, Y. Zhang, E. Wang, D. G. Schlom, C.-B. Eom, and X. Q. Pan, Revealing the role of defects in ferroelectric switching with atomic resolution, *Nat. Commun.* **2**, 591 (2011).
- [67] L. F. Zagonel, M. Bäurer, A. Bailly, O. Renault, M. Hoffmann, S.-J. Shih, D. Cockayne, and N. Barrett, Orientation dependent work function of in situ annealed strontium titanate, *J. Phys.: Condens. Matter* **21**, 314013 (2009).
- [68] A. J. Hartmann, M. Neilson, R. N. Lamb, K. Watanabe, and J. F. Scott, Ruthenium oxide and strontium ruthenate electrodes for ferroelectric thin-films capacitors, *Appl. Phys. A* **70**, 239 (2000).
- [69] S. Gariglio, N. Stucki, and J.-M. Triscone, Strain relaxation and critical temperature in epitaxial ferroelectric P(Zr_{0.20}Ti_{0.80})O₃ thin films, *Appl. Phys. Lett.* **90**, 202905 (2007).
- [70] G. Catalan, A. Janssens, G. Rispens, S. Csiszar, O. Seeck, G. Rijnders, D. H. A. Blank, and B. Noheda, Polar Domains in Lead Titanate Films Under Tensile Strain, *Phys. Rev. Lett.* **96**, 127602 (2006).
- [71] J. S. Shin, V. B. Nascimento, A. Y. Borisevich, E. W. Plummer, S. V. Kalinin, and A. P. Baddorf, Polar distortion in ultrathin BaTiO₃ films studied by in situ LEED I-V, *Phys. Rev. B* **77**, 245437 (2008).
- [72] T. Shimada, T. Ueda, J. Wang, and T. Kitamura, Hybrid Hartree-Fock density functional study of charged point defects in ferroelectric PbTiO₃, *Phys. Rev. B* **87**, 174111 (2013).
- [73] U. K. Mishra and J. Singh, *Semiconductor Physics and Design* (Springer, Dordrecht, 2008) p. 62.
- [74] A. Novikov, Experimental measurement of work function in doped silicon surfaces, *Sol.-St. Electron.* **54**, 8 (2010).
- [75] J. Becherer, *Electron Emission from Ferroelectric Thin Films and Single Crystals*, PhD thesis, Technische Universität Dresden, 2012, <https://d-nb.info/1068443650/34>, accessed March, 18, 2018.
- [76] J. O. McCaldin, T. C. McGill, and C. A. Mead, Correlation for III-V and II-VI Semiconductors of the Au Schottky Barrier Energy with Anion Electronegativity, *Phys. Rev. Lett.* **36**, 56 (1976).
- [77] J. Menéndez, A. Pinczuk, D. J. Werder, J. P. Valladares, T. H. Chiu, and W. T. Tsang, Band lineups at the GaSb-Al_xGa_{1-x}Sb heterojunction: Experimental evidence for a new common anion rule, *Solid State Commun.* **61**, 703 (1987).
- [78] C. M. Teodorescu, Image molecular dipoles in surface enhanced Raman scattering, *Phys. Chem. Chem. Phys.* **17**, 21302 (2015).
- [79] M. Iliut, C. Leordean, V. Canpean, C. M. Teodorescu, and S. Astilean, A new green, ascorbic acid-assisted method for versatile synthesis of Au-graphene hybrids as efficient surface-enhanced Raman scattering platforms, *J. Mater. Chem. C* **1**, 4094 (2013).
- [80] M. V. Ramana Murty, S. K. Streiffer, G. B. Stephenson, J. A. Eastman, G.-R. Bai, A. Munkholm, O. Auciello, and C. Thompson, In situ x-ray scattering study of PbTiO₃ chemical-vapor deposition, *Appl. Phys. Lett.* **80**, 1809 (2002).
- [81] C. Lichtensteiger, M. Dawber, N. Stucki, J.-M. Triscone, J. Hoffman, J.-B. Yau, C. H. Ahn, L. Despont, and P. Aebi, Monodomain to polydomain transition in ferroelectric PbTiO₃ thin films with La_{0.67}Sr_{0.33}MnO₃ electrodes, *Appl. Phys. Lett.* **90**, 052907 (2007).
- [82] L. Zhang, X. G. Chen, H. J. Gardner, M. A. Koten, J. E. Shield, and X. Hong, Effect of strain on ferroelectric field effect in strongly correlated oxide Sm_{0.5}Nd_{0.5}NiO₃, *Appl. Phys. Lett.* **107**, 152906 (2015).
- [83] X. G. Chen, X. Zhang, M. A. Koten, H. H. Chen, Z. Y. Xiao, L. Zhang, J. E. Shield, P. A. Dowben, and X. Hong, Interfacial charge engineering in ferroelectric-controlled Mott transistors, *Adv. Mater.* **29**, 1701385 (2017).